Argonne
NATIONAL LABORATORY

ANL-HEP-TR-09-9

Some Studies of Data Using the STAR Endcap Electromagnetic Calorimeter

High Energy Physics Division

About Argonne National Laboratory

Argonne is a U.S. Department of Energy laboratory managed by UChicago Argonne, LLC under contract DE-AC02-06CH11357. The Laboratory's main facility is outside Chicago, at 9700 South Cass Avenue, Argonne, Illinois 60439. For information about Argonne and its pioneering science and technology programs, see www.anl.gov.

Availability of This Report

This report is available, at no cost, at http://www.osti.gov/bridge. It is also available on paper to the U.S. Department of Energy and its contractors, for a processing fee, from:

U.S. Department of Energy
Office of Scientific and Technical Information
P.O. Box 62
Oak Ridge, TN 37831-0062
phone (865) 576-8401
fax (865) 576-5728
reports@adonis.osti.gov

ANL-HEP-TR-09-9

Some Studies of Data Using the STAR Endcap Electromagnetic Calorimeter

by
K. Krueger, H. Spinka, and D. Underwood
High Energy Physics Division, Argonne National Laboratory

January 2009

Some Studies of Data Using the STAR Endcap Electromagnetic Calorimeter

K. Krueger, H. Spinka, and D. Underwood
High Energy Physics Division
Argonne National Laboratory, Argonne, IL 60439

27 January 2009

Abstract

A series of studies was performed using data from the STAR detector at the Brookhaven National Laboratory's RHIC accelerator from collisions of protons at $\sqrt{s}$ = 200 GeV. Many of these involved the shower maximum detector (SMD) of the STAR endcap electromagnetic calorimeter (EEMC). Detailed studies of photon candidates from $\eta \rightarrow \gamma\,\gamma$ decay, and of γ + Jet inclusive data and simulated events were performed.

1. Introduction

STAR is a general purpose colliding beam detector (Ref. 1) operating at the RHIC accelerator. It consists of a large central tracking chamber (time projection chamber – TPC), an endcap electromagnetic calorimeter (EEMC – Ref. 2) on one end, and various other detectors. Collisions between heavy ions, deuterons and heavy ions, and between protons have been recorded and studied.

A physics process of interest for pp collisions is inclusive γ + Jet production, which is expected to be dominated by the $q\,g \rightarrow \gamma\,q$ subprocess. For incident longitudinally polarized proton beams, this process provides direct information on the intrinsic polarization of gluons in a polarized proton. However, backgrounds from other subprocesses producing π^0's or η's are sizeable.

Data were collected in spring 2006 with the STAR detector using beams of polarized protons at $\sqrt{s}$ = 200 GeV. Various subsets of these data were studied to understand the response of the EEMC to single photons and to learn how best to select γ + Jet inclusive events from the data. These studies were performed in collaboration with physicists from other STAR institutions.

This note begins with results from studies of individual events which were consistent with $\eta \rightarrow \gamma\,\gamma$ decays in order to find the response of individual photons. The opening angle of these decays is frequently large enough to separate the showers from the two photons; see Sec. 2. The response of the shower maximum detector (SMD), located within the EEMC, is studied in Sec. 3. The shape of showers in the SMD as a function of many parameters and for various data sets is evaluated. These data sets included two containing photon candidates from events consistent with $\eta \rightarrow \gamma\,\gamma$ decays, a data sample that will likely be used for the γ + Jet inclusives, and two Monte Carlo simulation sets. Section 4 gives results from studies of the amount of material traversed by photon candidates from their interaction point to the EEMC, and Sec. 5 describes some shower characteristics for events with identified charged particles. A summary of the most useful results concludes the note in Sec. 6.

2. Examination of Individual Events

Data from all 12 sectors for the EEMC towers, pre-shower1 and 2, post-shower, and the shower maximum detector (SMD) were evaluated "by hand." The events were selected by Pibero Djawotho (Ref. 3) from a set of 20 pp longitudinally polarized pp runs from 2006. He found $\eta \rightarrow \gamma\,\gamma$ candidates, selecting events with di-photon invariant masses between 0.45 and 0.65 GeV, and using tower and SMD seed thresholds of 0.8 GeV and 5 MeV, respectively. (A single tower or strip must pass the "seed threshold" before a cluster of towers or SMD strips can be formed. Additional towers or strips can be added to the cluster upon passing a lower threshold.) The signal to background ratio was less than 1:1.

The first 100 events were displayed on Pibero's website (Ref. 3). The first 25 of these events were analyzed. In addition, Will Jacobs selected 23 out of the 100 that appeared more likely from $\eta \rightarrow \gamma\,\gamma$ decays, and these 23 events were also analyzed for comparison.

Selecting events with energy greater than about 2 GeV (56 and 48 towers in the first 25 and Will's sample, respectively), and investigating the energy deposited in the corresponding pre-shower detector led to the following conclusions:

- There is weak evidence for a correlation of pre-shower1 and pre-shower2 energies corresponding to single tower "clusters".
- Will's pre-shower1 energy distribution seems to be more concentrated at zero energy than the sample from the first 25 events ($\langle E \rangle \sim 1.9$ vs. 3.8 MeV – see Fig. 1).
- Similarly, $26/48 = 0.54 \pm 0.07$ and $16/56 = 0.29 \pm 0.06$ of the towers had pre-shower1 energy equal to zero for Will's and the first 25 events, respectively.

These conclusions all suffer from the small number of events analyzed.

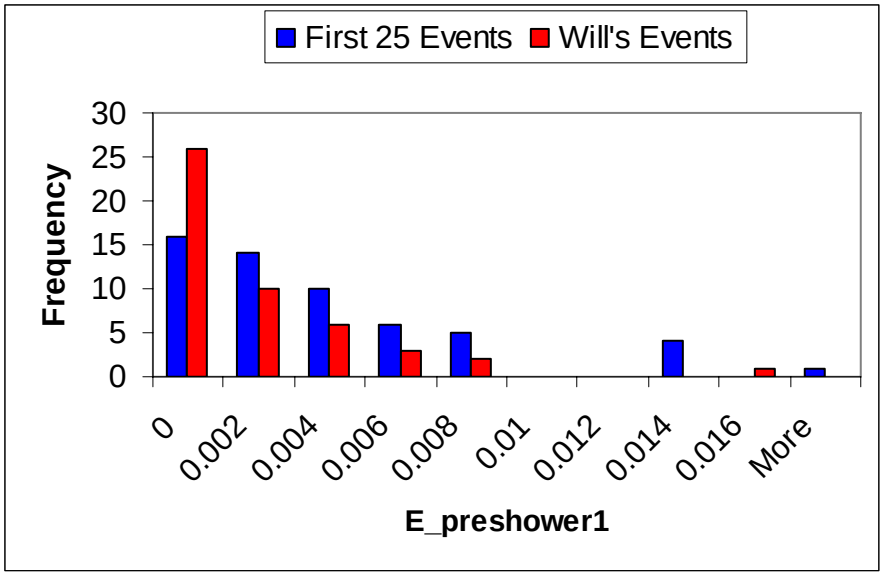

Fig. 1. Histogram of the energy (in GeV) deposited in the pre-shower1 detector associated with towers containing energy of at least 2 GeV. Data are shown for the first 25 events and for Will's events.

Searches were made for correlations involving the tower energy (selected to have more than about 2 GeV, as above), the corresponding pre-shower counter energies, and the SMD shower "width." The likely SMD scintillator strips corresponding to the tower with the highest energy were identified in the same sector as the tower. (Note that the detailed correspondence of SMD strip numbers and towers was not checked.) The SMD width was then estimated at the base of the energy distribution, with at least one strip having zero energy. The average of U and V widths was performed, but the estimates were somewhat subjective. The results of the searches were:

- A possible correlation of SMD width and pre-shower1 or tower energy may be present in the first 25 events.
- There is also weak evidence for a correlation of pre-shower1 and pre-shower2 energies in the first 25 events.
- Including data from all sectors in an event, there is a correlation of the number of nonzero energy towers and of nonzero energy pre-shower1 counters for both types of events. The correlations appear to be the same – see Fig. 2.

These observations need to be compared to appropriate simulations to investigate whether they agree.

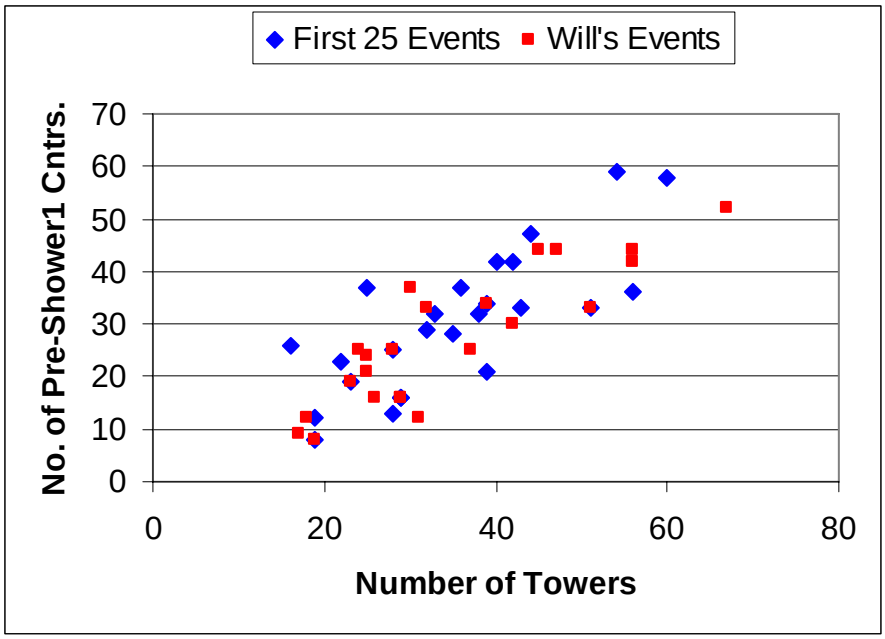

Fig. 2. Correlation of the number of nonzero energy pre-shower1 counters and nonzero energy towers from all sectors in the η → γ γ decay events. Little difference is observed between the first 25 events or the events selected by Will Jacobs.

Sectors other than those with the η candidate were investigated. The number of clusters of SMD strips with energies corresponding to ~ 1 "mip" (minimum ionizing particle) or to larger energies was recorded for each event. The "mip" events often involved two adjacent strips. These "mip" and large energy cluster events occurred approximately uniformly throughout the EEMC and the average number of sectors without any energy was 4 (out of 12) for the first 25 events. The location of the "mip" and large cluster events relative to the η candidate sector was recorded – see Fig. 3. No strong dependence on sector difference is observed. Note that the number of events with sector difference 6 was doubled, since only one sector contributed there, while two contributed to the other differences.

Finally, in a few cases, isolated strips with more than 4 "mips" energy deposited were observed. There were 5 strips that were high in at least one event from the first 25 events, and a total of 12 strips in the full sample of 100 events. Six of these strips were eventually identified as "bad" on the basis of status tables, online (Panitkin) plots of the frequency of hits for each strip, and plots of the ADC and energy distributions for each strip. No problems could be identified for the remaining six events. The origin of these isolated strips with sizeable energy is unknown. It is also not known whether such events are in simulations or arise from some additional background source.

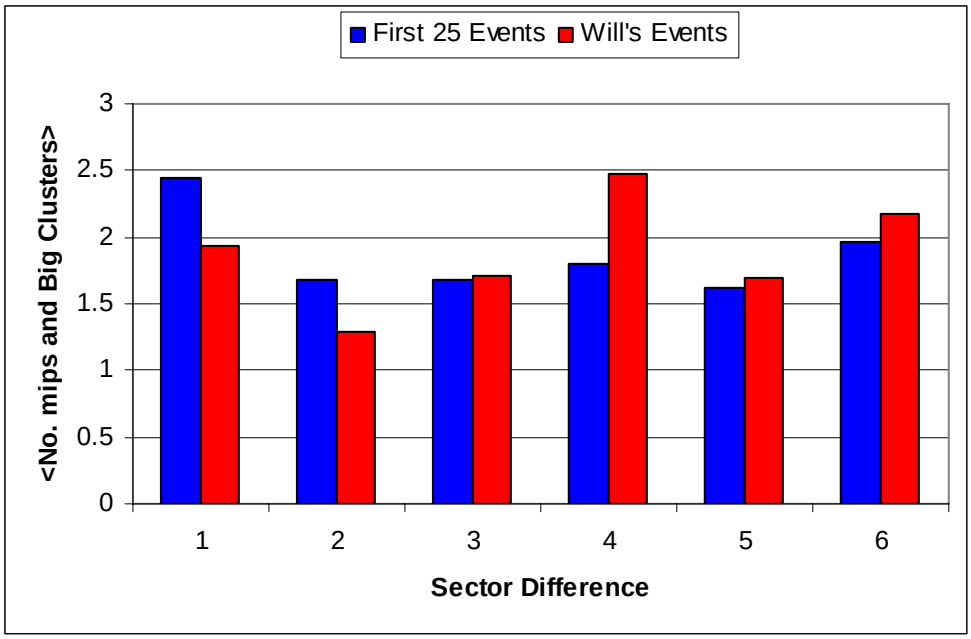

Fig. 3. The average number of "mip" and large cluster events as a function of sector difference from the η candidate sector is plotted. The number with sector difference 6 was doubled to correspond to the same number of sectors per difference. No strong dependence on sector difference is seen.

3. SMD Shower Shape Studies

a. General Features from Pibero's Sample

A number of studies were performed using a sample of 927 photon candidates consistent with $\eta \rightarrow \gamma\,\gamma$ decays obtained by Pibero Djawotho (Ref. 4). A total of 44 runs from the 2006 longitudinally polarized pp run period were analyzed. The steps to obtain these candidates included: a) a single or seed tower with $p_T > 0.8$ GeV/c, b) no TPC track pointing toward that tower (such tracking was available only to $\eta <\sim 1.6$), c) the energy must be > 2 MeV for the U and V strips with the maximum energy within the seed tower area, d) the intersection of the maximum energy strips must lie within a fiducial area of 70% of the area of the seed tower (the strips usually extend far beyond the towers), e) the projected line from the interaction point to the SMD intersection remains within the seed tower, f) 70% of the summed energy in ±20 strips about the maximum energy strip was within ±5 strips for both U and V planes, g) the energy asymmetry of the summed energy for the U and V planes was less than 0.2, h) a "point" was created with the seed tower energy and the SMD position; the invariant mass of a pair of points was required to fall within 0.4 – 0.6 GeV, and then the data for the points were recorded as photon candidates in a .txt file. The results were analyzed with a c program within the CERN Root framework and are reported here.

Some characteristics of the event sample are shown in Fig. 4. The photon candidate energies from the towers range from about 2 to 25 GeV, while the transverse energy is predominantly below 5 GeV. The pseudo-rapidity distribution is peaked near the center of the EEMC acceptance at $\eta \sim 1.5 - 1.6$, and the phi distribution is flat, as expected. Figure 5 shows an overlay of the U and V centers for the candidates – the effect of requirements d and e above can be seen as the empty areas between the tower centers. The energies of the SMD U and V planes (summed over all strips!) are well correlated, possibly related to requirement g above, but the SMD and tower energies are poorly correlated (see Fig. 6). This may be due to gamma conversions at various positions before the calorimeter, so that the shower development was at different stages at the SMD depth for different events.

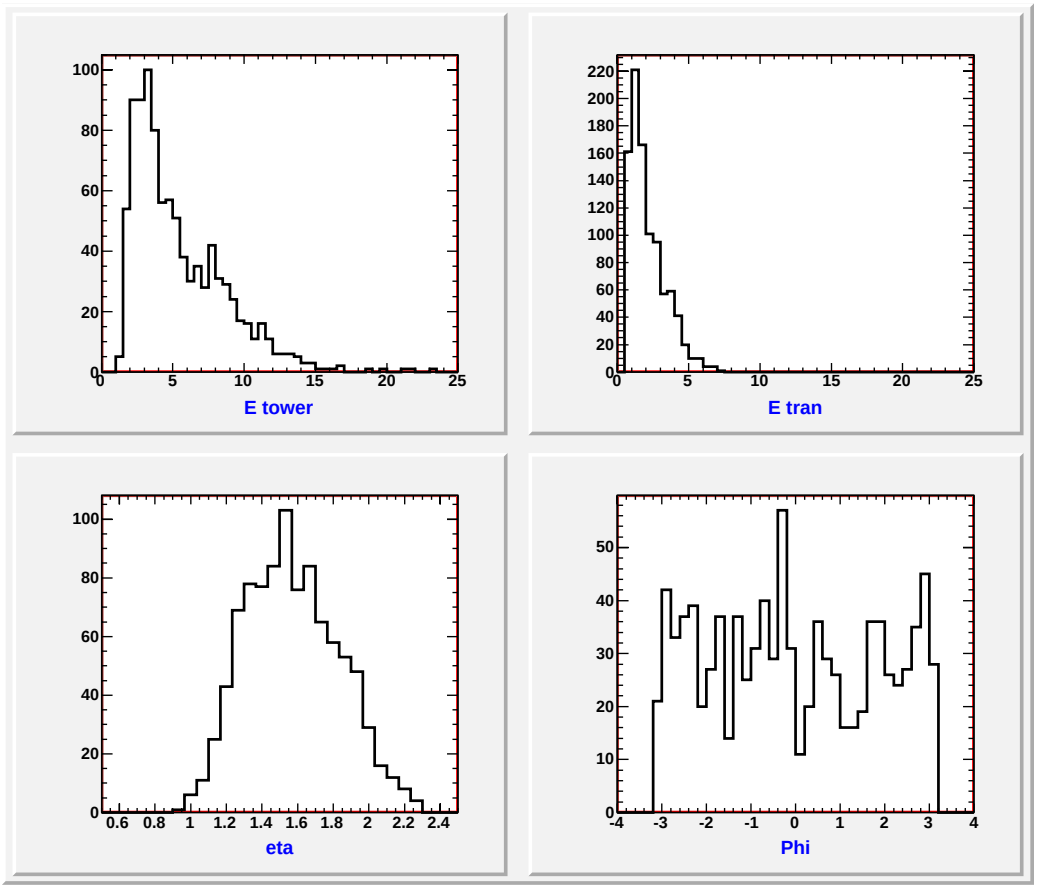

Fig. 4. Some general characteristics of the photon candidates from Pibero's events consistent with $\eta \rightarrow \gamma\,\gamma$ decays are plotted. The tower energy is given in the upper left, the transverse energy in the upper right, the pseudo-rapidity corrected for the interaction point in the lower left, and the phi distribution in the lower right panel. The energies are in GeV, and phi is in radians.

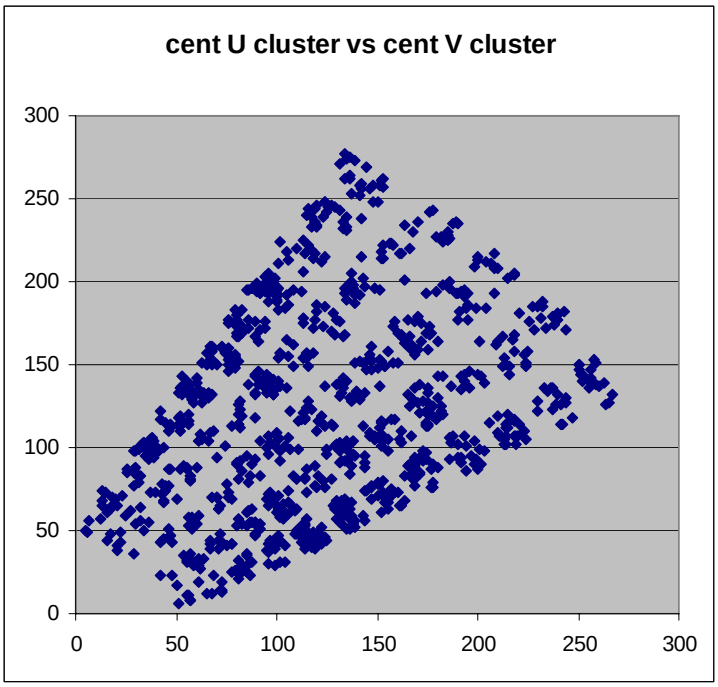

Fig. 5. Plot of the location of the intersection of the SMD U and V strip with maximum energy within the seed tower, with all sectors overlain. The intersection points cluster near tower centers, due to requirements in the event selection.

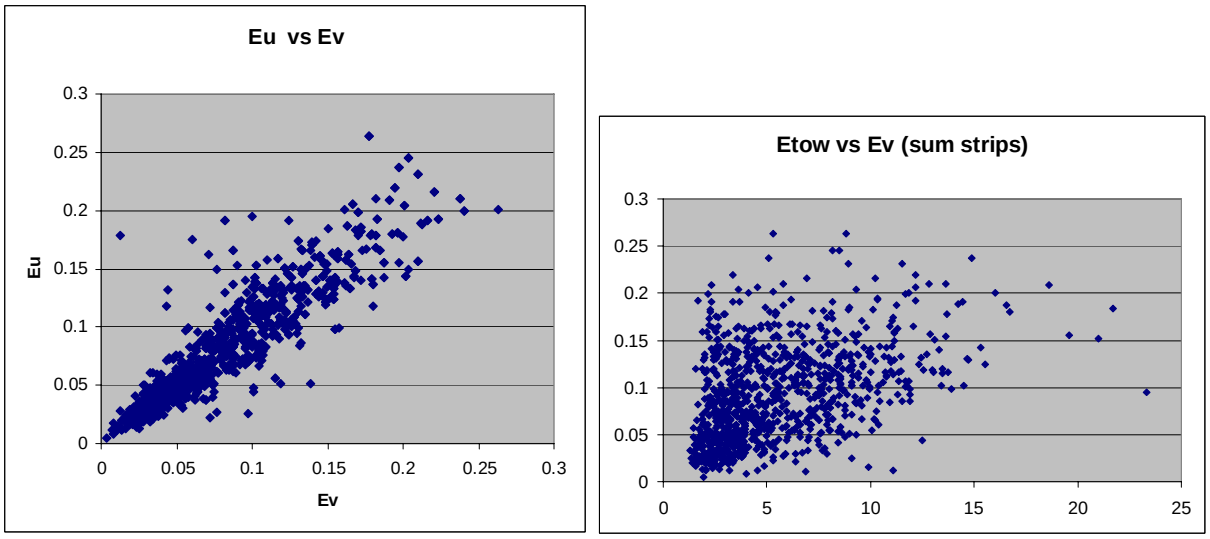

Fig. 6. Correlations of SMD U vs. V energies summed over all strips in each plane, and of the summed SMD V energy vs. tower energy. All energies are in GeV. A strong correlation is seen between U and V, but not between the SMD and tower energies.

The summed energies for all strips in each SMD plane are shown in Fig. 7. In addition, summing the energies for all events as a function of strip number produced the shower shapes also given in Fig. 7. The uncertainty on the shower shape width is approximately $\delta(\text{RMS}) \sim (\text{RMS})/\sqrt{(N=927)} \sim 0.1$. The widths in the U and V planes can be seen to be identical within statistical uncertainties.

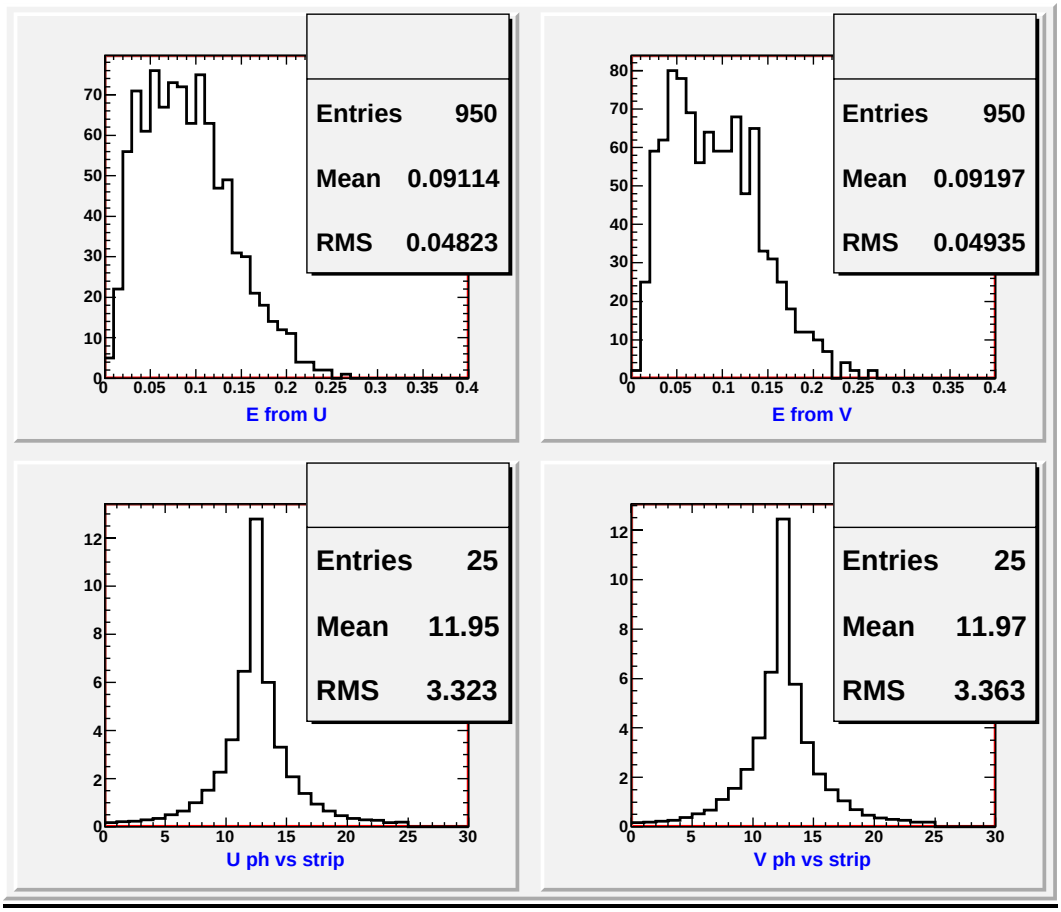

Fig. 7. Additional general characteristics of Pibero's photon candidate sample. The upper histograms show the summed SMD energy in GeV for all strips in each plane, and the lower two give the SMD shower shape summed over all 927 candidates.

A number of studies were performed with the SMD shower shapes defined as above. In the EEMC construction, the SMD can have three possible orderings as seen by entering particles from the intersection point: 1) U, V, and spacer, 2) spacer, U, and V, and 3) V, spacer, and U. The observed shower RMS values for the three cases were found to be 3.16, 3.29, 3.52 strips for U and 3.45, 3.55, 3.07 strips for V, respectively. Thus the shower width increases as the SMD distance increases from the start of the shower by about 10 – 15%. Note that the uncertainties on the widths are approximately $\pm 0.1 * \sqrt{3} = 0.17$ strips, since the events were split into three roughly equal groups.

The SMD shower widths were also tested for dependence on tower energy, SMD energy, and pseudo-rapidity. Since the 927 events were split among three bins of roughly equal numbers here also, the uncertainties on the widths quoted are approximately 0.17. It was observed that the shower width was perhaps weakly correlated with tower energy (RMS = 3.40 strips for E_{Tower} = 0 – 4 GeV, 3.31 for 4 – 8 GeV, and 3.28 for 8 – 35 GeV). The width showed a slight increase with SMD energy (RMS = 3.21 strips for E_{SMD} = 0 – 0.12 GeV, 3.30 for 0.12 – 0.24 GeV, and 3.40 for 0.24 – 0.5 GeV). Finally, there was no obvious trend for shower width vs. pseudo-rapidity (RMS = 3.40 strips for η = 0.5 – 1.4, 3.27 for η = 1.4 – 1.8, and 3.34 for η = 1.8 – 2.5).

The correlation of the pre-shower counter energies is shown in Fig. 8, where a considerable scatter is observed. The energy in pre-shower2 is roughly double that in pre-shower1 on average. A considerable correlation is observed between the RMS width in the SMD planes and the pre-shower1 energy, as seen in Fig. 9, even considering the estimated uncertainties on each point. Showers that convert before the EEMC and are more developed before reaching the EEMC will be wider at the SMD. Photons converting in the TPC support wheel will also cause a wide shower, and will be eliminated by requiring the pre-shower1 energy to be zero. A plot of the average U and V SMD shower width in strips as a function of tower energy for pre-shower1 energy equal to zero is also shown in Fig. 9, and the width decreases with increasing energy.

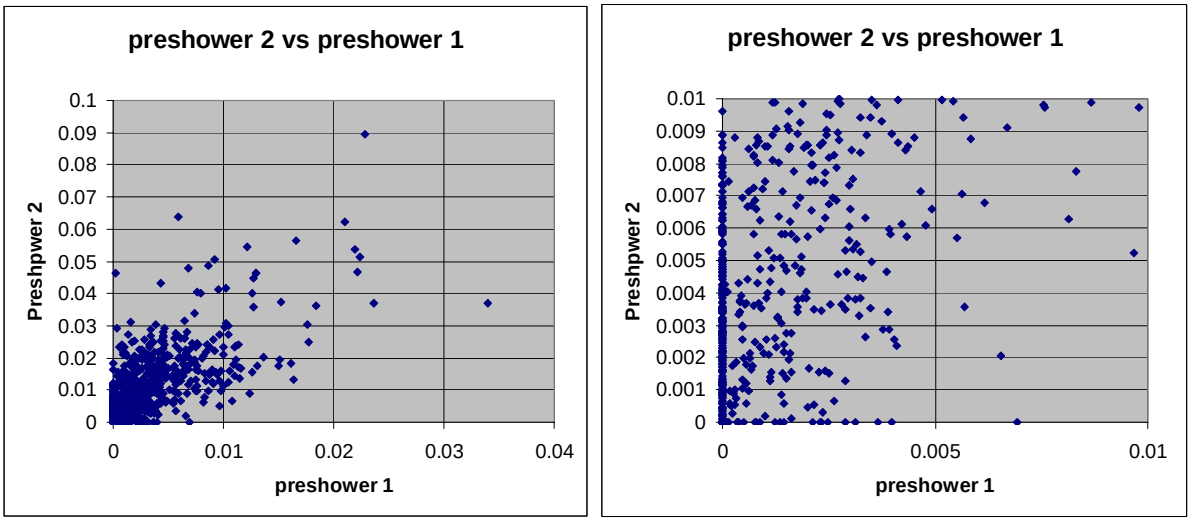

Fig. 8. Correlation of energies in pre-shower 2 vs. pre-shower1 counters in GeV. A strong correlation is not observed. The figure on the right has an expanded scale compared to the one on the left.

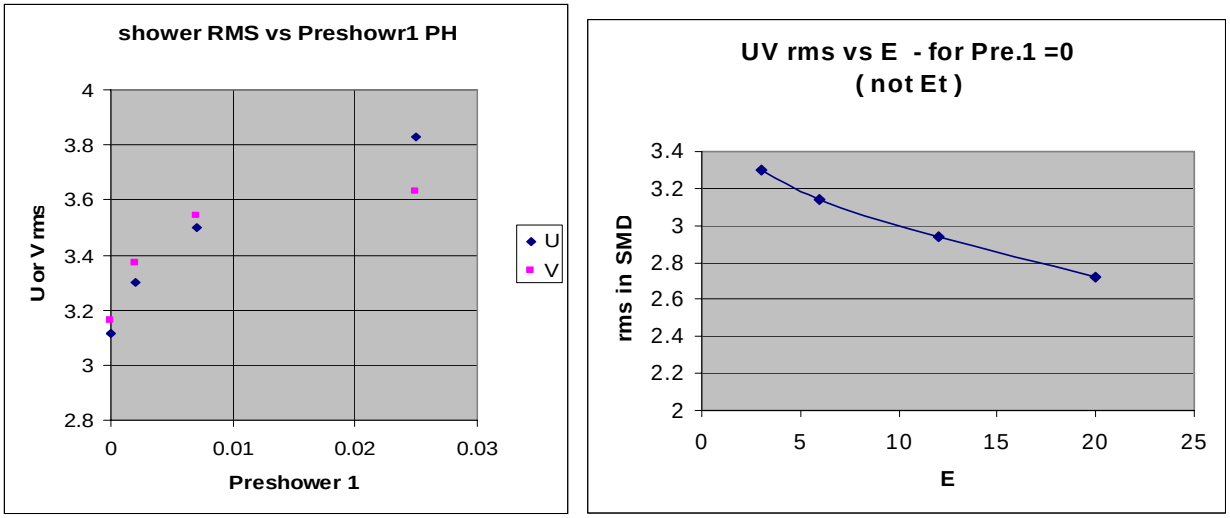

Fig. 9. RMS SMD shower width for U and V planes as a function of pre-shower1 counter energy in GeV (left). A significant increase with energy is observed. For pre-shower1 energy equal to zero, the average SMD width in strips is plotted as a function of tower energy in GeV (right).

b. General Features from Will's Sample

Following the work with Pibero's photon candidates, Will Jacobs generated a larger sample of such candidates also consistent with $\eta \rightarrow \gamma\,\gamma$ decays (3334 "photons" – see Ref. 5). He used 425 runs taken during the 2006 longitudinally polarized pp periods. There were differences from the requirements imposed by Pibero. Some of these included: a) the maximum energy SMD strip must contain > 5 MeV instead of > 2 MeV, b) no strips that were "dead" due to hardware problems were allowed in a 7 strip cluster, c) only one or two SMD clusters were permitted in each (U, V) plane, d) the minimum allowed separation between two clusters in a SMD plane was 20 strips, e) Pibero's conditions d and e, involving the fiducial area of the tower and the projected track remaining within the tower, were not required, f) no SMD energy asymmetry cut similar to Pibero's condition g was applied, g) a cut of $p_T > 6$ GeV/c was made, and h) the invariant mass of two photon candidates was required to fall between 0.45 and 0.65 GeV. In particular, the requirement that 70% of the summed energy within ±20 strips about the maximum energy strip was within ±5 strips for both U and V planes was also imposed (Pibero's condition f). Clusters of 3 x 3 towers were used to determine the energy of the photon.

Some general characteristics of the event sample are shown in Fig. 10 (see Fig. 4 for a comparison to Pibero's sample). The tower and transverse energies extend to higher energies, and also have a cutoff at lower energies due to condition g above. The pseudo-rapidity and phi distributions look similar to Pibero's results. The distribution of SMD summed energies from the strips is similar except the low energies are cut off, and the average shower shapes are perhaps a bit narrower (3.20 vs. 3.34) – see Figs. 11 and 7.

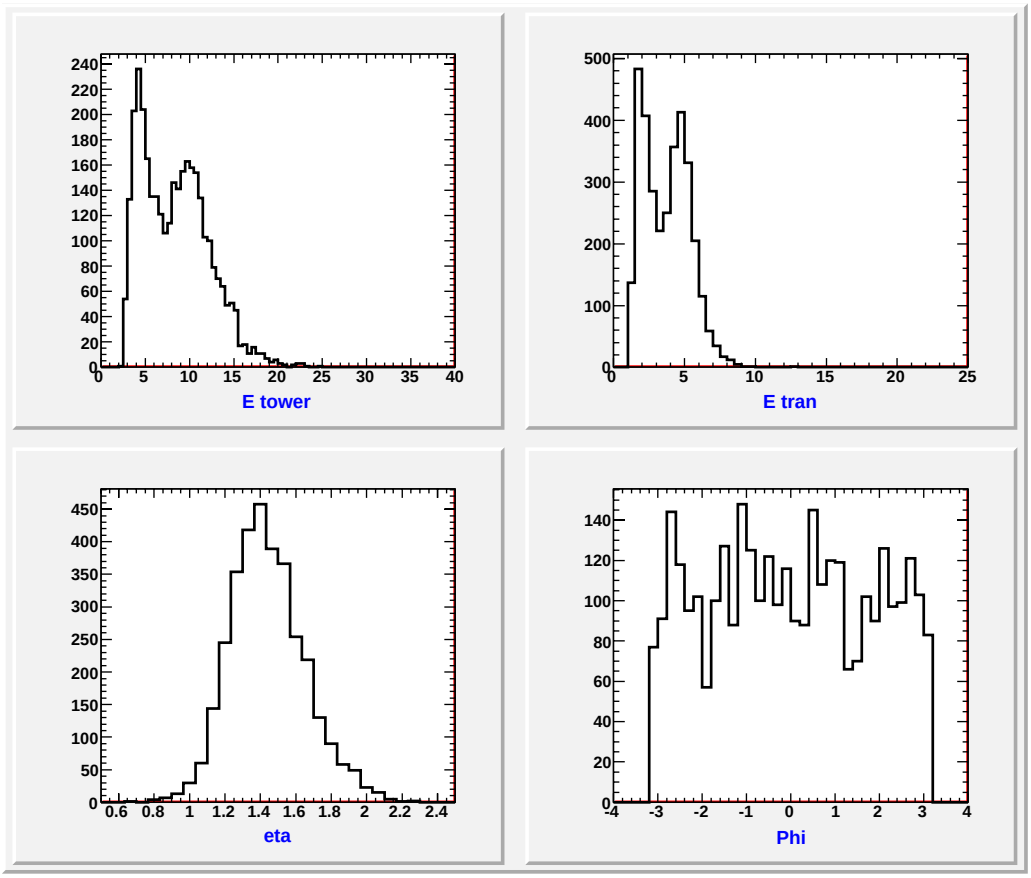

Fig. 10. Some general characteristics of the photon candidates from Will's events consistent with $\eta \rightarrow \gamma\,\gamma$ decays are plotted. The tower (3 x 3 cluster) energy is plotted in the upper left, the transverse energy in the upper right, the pseudo-rapidity in the lower left, and the phi distribution in the lower right panel. The energies are in GeV, and phi is in radians.

Some of the studies with Pibero's photon candidates were repeated. For the case with the SMD depth orderings, the observed SMD shower widths were 2.92, 3.21, and 3.48 strips for U, and 3.33, 3.53, and 2.95 strips for V for the 1, 2, and 3 orderings given above in Sec. 3.a. The uncertainties on the widths are approximately ±0.10 strips, and the widths are generally similar to those observed previously. In this case, the statistical significance of the differences is considerably improved. Thus, the width increases with the depth of the SMD plane in the EEMC.

The correlation of summed energy in the U and V planes of the SMD is shown in Fig. 12. It is to be compared to the same result from Pibero given in Fig. 6, which appears narrower, possibly because of his condition on the SMD energy asymmetry (requirement g). The similar correlation for energy summed over the ±12 strips about the strip with the maximum energy is also shown in Fig. 12, and an even larger spread is apparent.

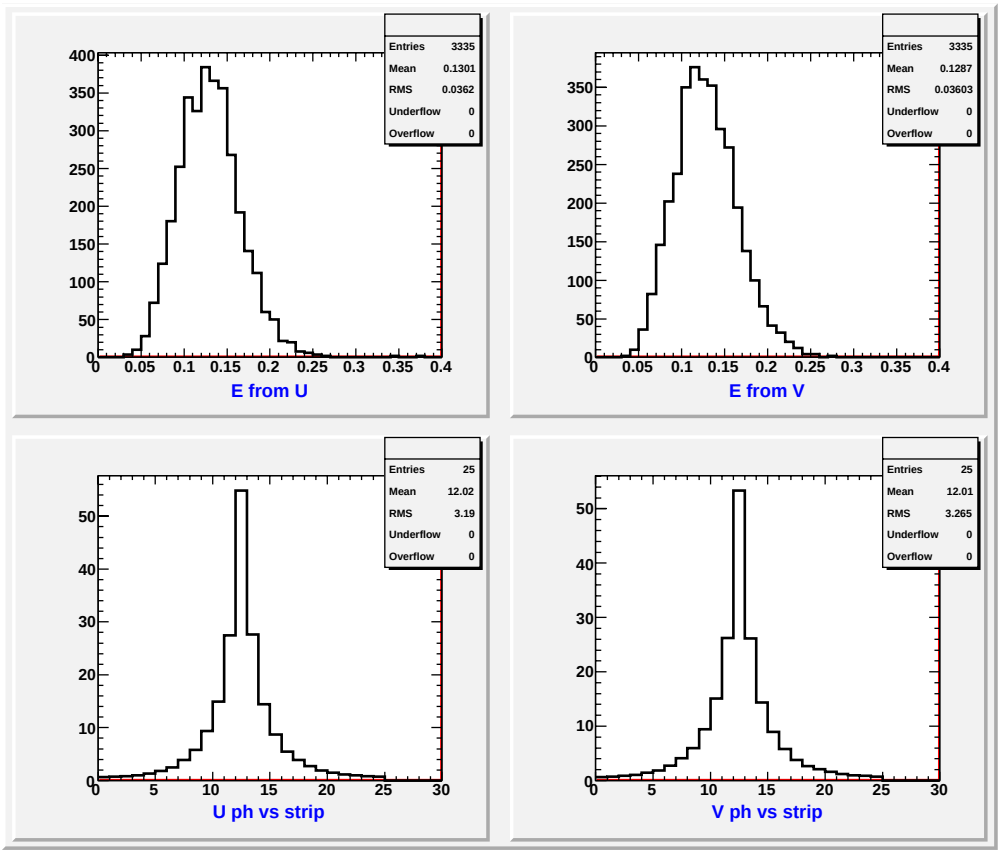

Fig. 11. Additional general characteristics of Will's photon candidate sample. The upper histograms show the summed SMD energy in GeV for all strips in each plane, and the lower two give the SMD shower shape summed over all 3334 candidates. Comparing to Fig. 7, the SMD energies are cut off below about 0.05 GeV, and the shower shapes are somewhat narrower.

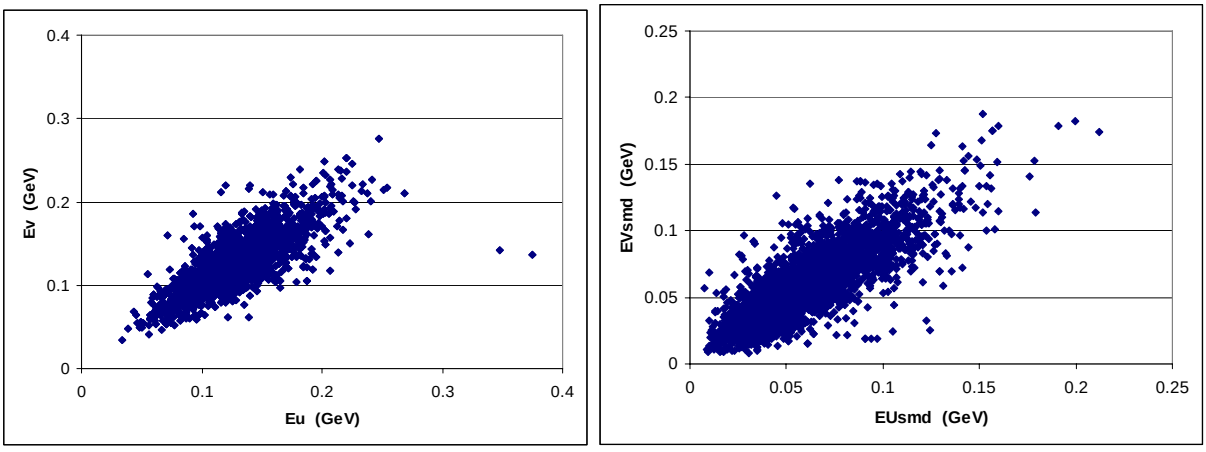

Fig. 12. Correlations of summed energy in V vs. U SMD planes (left) and in ±12 strips about the strip with maximum energy (right) are plotted for Will's candidate photons. All energies are in GeV. The left plot should be compared to Pibero's results in Fig. 6.

An unusual feature of Will's photon candidates is the two peaks in the tower cluster and transverse energy distributions of Fig. 10. There is perhaps also a hint of a second peak in the tower energy distribution for Pibero's candidates in Fig. 4. These may be caused by preferentially selecting asymmetric $\eta \rightarrow \gamma\,\gamma$ decays, since it appears that both photons were always retained in Will's sample and frequently for Pibero's photon candidates. Furthermore, the energy asymmetry $z_{\gamma\gamma} = |E_{\gamma,1} - E_{\gamma,2}|/(E_{\gamma,1} + E_{\gamma,2})$ is peaked near 0.4 – 0.5 in Will's data before making his invariant mass cut; see Fig. 5 of Ref. 6. The invariant mass and $z_{\gamma\gamma}$ distributions of Will's events are shown in Fig. 13 (pairs of photon candidates consistent with an $\eta \rightarrow \gamma\,\gamma$ decay occur sequentially in Will's data set).

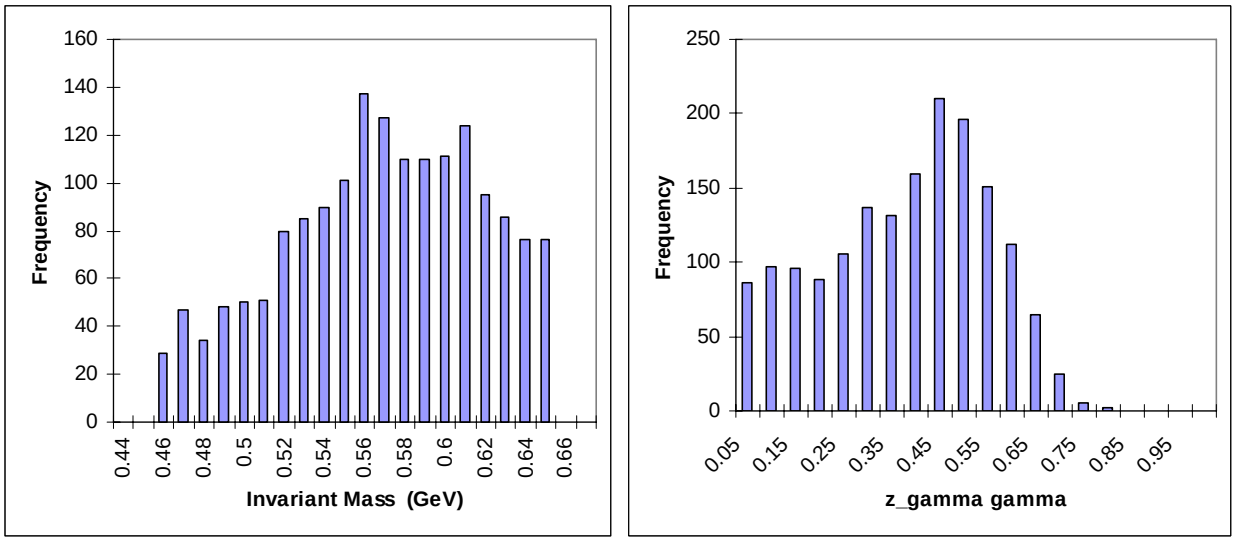

Fig. 13. Invariant mass and $z_{\gamma\gamma}$ distributions are plotted for Will's photon candidates. The η peak is visible in the invariant mass histogram. The peak in the $z_{\gamma\gamma}$ histogram may be the cause of the double peaks in the tower and transverse energy distributions in Fig. 10.

c. Additional Comparisons of Pibero's and Will's Results

A different definition of shower shape was used for some studies. In the analyses of Sec. 3.a and 3.b, the sum of energies for each strip within ±12 of the one with maximum energy was computed. Thus, the contribution of each photon candidate to the shower shape was weighted by the summed energy in the 25 strips. The alternate approach first found the energy weighted mean strip within ±12 strips of the one with maximum energy. Then the area of the 25 strips was normalized to unity, the distributions aligned to have the weighted mean strip centered, and an average shape computed.

Using this alternate shower shape definition, a comparison of the mean shower shape and RMS variation as a function of strip position for Pibero's and Will's photon candidates is shown in Fig. 14. These can be seen to be very nearly identical, although the RMS values for Pibero's sample are slightly larger than for Will's sample. The same is also true when comparing restricted tower energy ranges (0-4, 4-8, 8-35 GeV, not

shown) – the shower shapes are nearly identical, but the RMS distributions are slightly wider for Pibero for 0-4 GeV, and slightly narrower for the other two energy bins. Figure 15 plots the shower shapes and RMS values for four tower energy ranges for Will's photon candidates. Very little change in shower shape is observed with energy. The RMS values decrease with energy, but seem to change relatively slowly above 8 GeV.

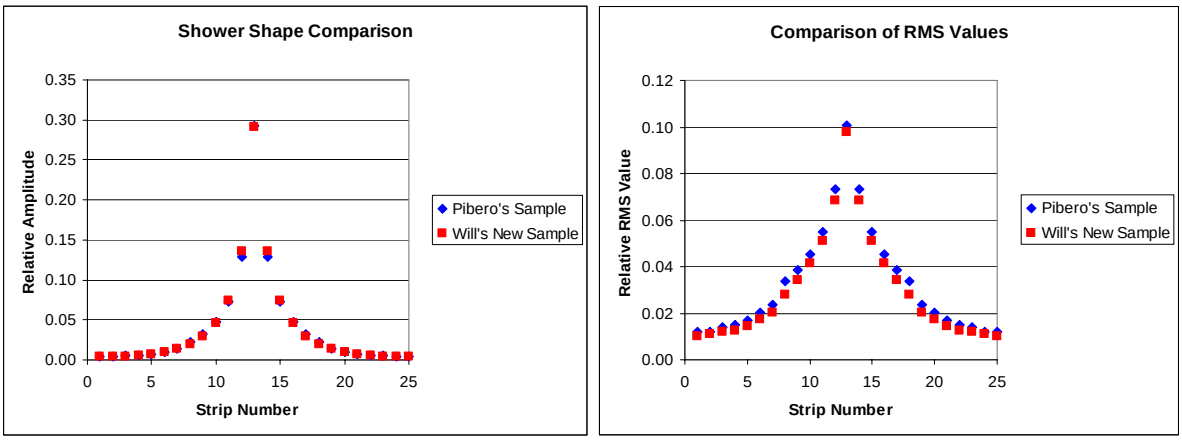

Fig. 14. Comparisons of the relative amplitude and RMS variation for the photon candidates of Pibero and Will are shown. These plots indicate that the two samples are quite similar.

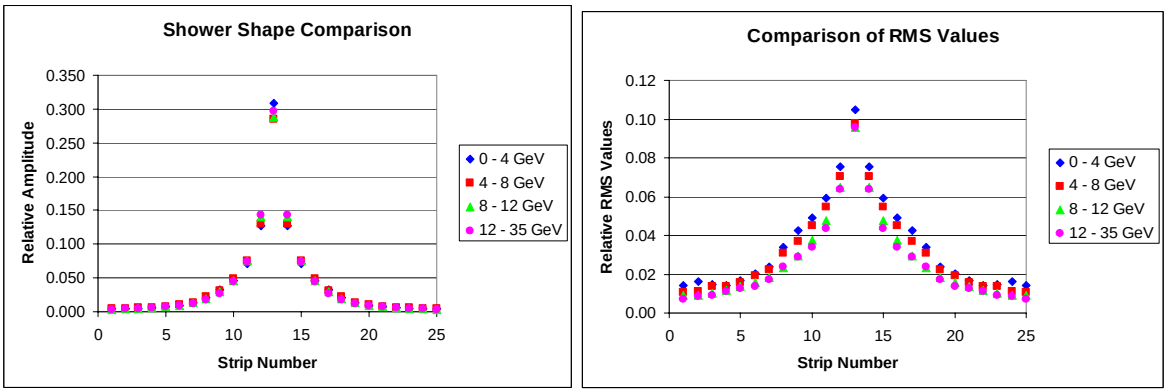

Fig. 15. Comparisons of relative amplitudes and RMS variations as a function of strip number for Will's photon candidates and four tower energy bins are shown. The shower shapes are nearly identical, but the RMS values decrease with increasing tower energy.

A comparison of the shower shape and RMS variation as a function of pseudo-rapidity was also performed, as shown in Fig. 16. Very little difference is observed. As noted by Scott Wissink (Ref. 7), the width of the shower shape distribution is expected to decrease at larger pseudo-rapidity due to geometric effects. The average U and V plane widths were found to be 3.252 ± 0.061 strips for $\eta = 1.0 - 1.4$, 3.227 ± 0.067 strips for $\eta = 1.4 -$

1.6, and 3.157 ± 0.086 strips for η = 1.6 – 2.0. The expected ratio of widths for the first to third range was 1.054, and the observed value was 1.030 ± 0.034.

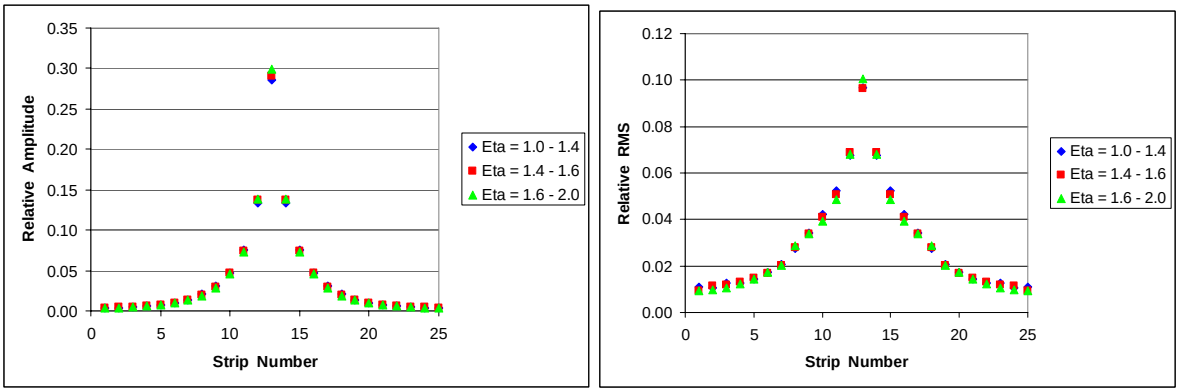

Fig. 16. Comparisons of relative amplitudes and RMS variations vs. strip number for Will's photon candidates at three pseudo-rapidity ranges. The distributions appear quite similar.

Some additional calculations were made to supplement analyses performed by other STAR collaborators. The pseudo-rapidity distribution of the photon candidates was determined for three pre-shower energy conditions (Pre1=0, Pre2=0), (Pre1=0, Pre2>0), and (Pre1>0, Pre2>0). The mean, RMS values, and numbers of events for Pibero's candidates were (1.54, 0.25, 153), (1.51, 0.25, 204), and (1.60, 0.26, 546), respectively. For Will's photon candidates, the results were (1.446, 0.223, 605), (1.426, 0.210, 756), and (1.449, 0.208, 1860), respectively. Very little dependence on pre-shower energy conditions was observed in the pseudo-rapidity distributions, though Pibero's photons were at slightly larger pseudo-rapidity on average than Will's photons. (There were also a few events with Pre1>0, Pre2=0 – 24 for Pibero's and 113 for Will's sample.)

From these numbers, the fraction of events with pre-shower1 energy equal to zero was determined to be [(153+204) / (153+204+546+24)] = 0.385 ± 0.016 and [(605+756) / (605+756+1860+113)] = 0.408 ± 0.009 for Pibero's and Will's candidates, respectively. However, a calculation of this ratio from the "known" material suggests that a larger value should be observed if only single photons were present. This is discussed further in Sec. 4.

d. Comparisons to γ + Jet Inclusive Candidate Data and Simulations

A comparison was made between properties of five "photon" samples: Pibero's and Will's candidates consistent with $\eta \rightarrow \gamma\,\gamma$ decays (data), a set of photon candidates from Ilya Selyuzhenkov, Monte Carlo simulated events from inclusive γ + Jet production with the γ SMD shower shape replaced by that from one of Will's photon candidates, and Monte Carlo events from inclusive γ production provided by Jason Webb.

Ilya's candidates were taken from the run 6 di-jet event sample. These events satisfied the following conditions: a) the ratio of electromagnetic to total energy in one jet (designated jet 1) was required to be larger than 0.9, or $E_{EM} / E_{TOT} > 0.9$, b) the same ratio for jet 2 was required to be $E_{EM} / E_{TOT} < 0.9$, c) there were no charged tracks from the TPC associated with jet 1, d) the two jets were nearly coplanar, $\cos (\varphi_1 - \varphi_2) < -0.8$, e) the transverse momentum for the two jets was $P_{T,1} > 7$ GeV/c and $P_{T,2} > 7$ GeV/c, and f) the fraction of energy in a 3 × 3 tower cluster centered on the EEMC tower with the highest energy compared to the total energy in jet 1 was $E_{CLUSTER} / E_{TOT} > 0.9$. The jet energy, E_{TOT} , was measured in a (η, φ) radius of 0.7 about the tower with the highest energy. The inclusive γ + Jet Monte Carlo events were subjected to the same conditions as for Ilya's sample above.

Two simple comparisons involved ratios of events selected on the basis of pre-shower counter energy. In the analysis of these counters, the mean ADC pedestal and its RMS width (σ_{ped}) were determined. Then, these pre-shower counters were considered to have nonzero energy only if their ADC values were more than $3 * \sigma_{ped}$ above the mean pedestal value. The ratios below will be given for Pibero's and Will's photon candidates, Ilya's events, the inclusive γ + Jet Monte Carlo photons, and the inclusive γ Monte Carlo events. The number of events in the categories (Pre1=0, Pre2=0), (Pre1=0, Pre2>0), (Pre1>0, Pre2>0), and (Pre1>0, Pre2=0) for Ilya's events were (309, 1023, 20593, 188), for Ilya's Monte Carlo events were (769, 1155, 4097, 131) and for Jason's Monte Carlo events were (111, 150, 599, 31), respectively.

The first ratio was the fraction of events with zero pre-shower1 energy,

Frac.(Pre1=0)	= #(Pre1=0) / [#(Pre1=0) + #(Pre1>0)]	
	= 0.385 ± 0.016, 0.408 ± 0.009	Pibero, Will
	= 0.060 ± 0.002	Ilya
	= 0.313 ± 0.006, 0.293 ± 0.015	Monte Carlo

respectively. These results show that the ratio from photon candidates from $\eta \rightarrow \gamma \gamma$ decays agree, and are larger than the two Monte Carlo ratios, which are also consistent. All four of these give significantly larger ratios than those from Ilya's data. Two possible explanations include considerable additional material in the actual detector compared to the simulations, or the dominance of processes other than γ + Jet inclusives in the recorded data. If only one photon was typically within the 3 × 3 tower cluster, then the difference between the E_{Pre1}=0 fraction of 0.06 and 0.31 would correspond to roughly 1.28 radiation lengths of material on average; see Sec. 4.

Another ratio that can be computed from the number of events is the conversion probability between the pre-shower1 and pre-shower2 counters, defined as

Conv. Prob.	= #(Pre1=0, Pre2>0) / #(Pre1=0)	
	= 0.571 ± 0.026, 0.555 ± 0.013	Pibero, Will
	= 0.768 ± 0.012	Ilya

$= 0.600 \pm 0.011, 0.575 \pm 0.031$ Monte Carlo

respectively. The results from Pibero's and Will's candidates are consistent, and from the two Monte Carlo samples are consistent, and these are all smaller than the ratio from Ilya's events.

The differences between Ilya's data ratios and those from either the Monte Carlo photons or the photon candidates consistent with $\eta \rightarrow \gamma\,\gamma$ decays are of concern, since these ratios do not involve details of the transverse shower shapes. One possibility is that Ilya's sample contains a significant number of particles other than photons, including neutral hadrons and charged particles (where the TPC efficiency is poor at forward angles) or more photons on average than the other samples. In particular, γ + Jet inclusive events may not dominate Ilya's data sample.

The conversion probability was computed in pseudo-rapidity bins of 0.2 from 1.0 – 2.0 and the results plotted in Fig. 17 for Will's and Ilya's data. Using the known material between the pre-shower1 and pre-shower2 counters, approximately 0.87 radiation lengths, and assuming single photons originating at the center of STAR, then the computed conversion probabilities at pseudo-rapidity 1.0 and 2.0 are about 0.589 and 0.504, respectively. A line is shown in Fig. 17 corresponding to this calculation, and the results follow closely Will's data. The conversion probability drops at larger η as the photons enter the EEMC closer to normal incidence. On the other hand, Ilya's data sample rises slightly with pseudo-rapidity, possibly from additional particles or photons per 3×3 tower cluster.

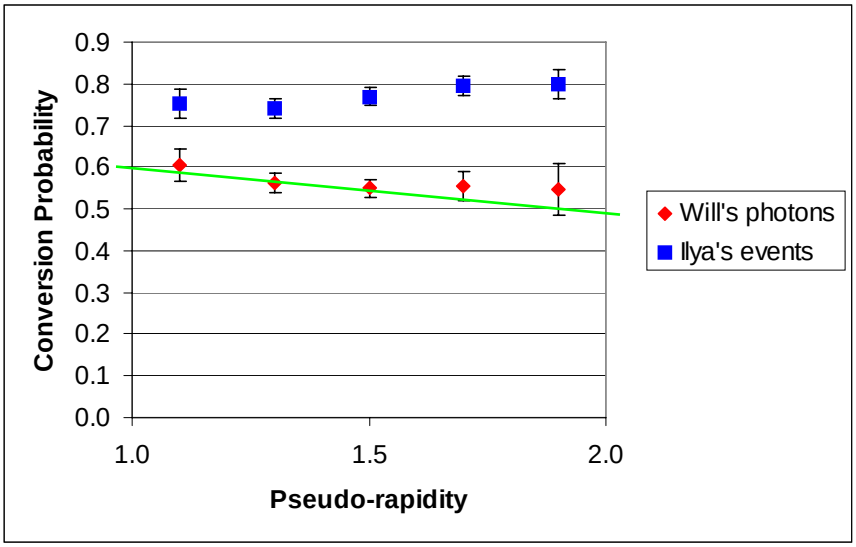

Fig. 17. Conversion probability is plotted as a function of pseudo-rapidity for Will's photon candidates and Ilya's events. The line shows the expected behavior for single photons.

The conversion probability was also computed as a function of the number of SMD strips with non-zero energy within ±12 strips of the one with maximum energy. Figure

18 shows the results from several photon samples. Ilya's Monte Carlo and Will's events seem to show the same behavior as a function of the number of strips. This may not be surprising, as Ilya's Monte Carlo events have the SMD shower shape replaced by one from Will's sample. However, Will's and Ilya's samples agree at small and large number of strips, but diverge in between. (The mean number of strips is larger for Ilya's that for Will's sample, giving a larger average conversion probability noted earlier.) There is also an indication that the >8 GeV events may have a slightly smaller conversion probability on average.

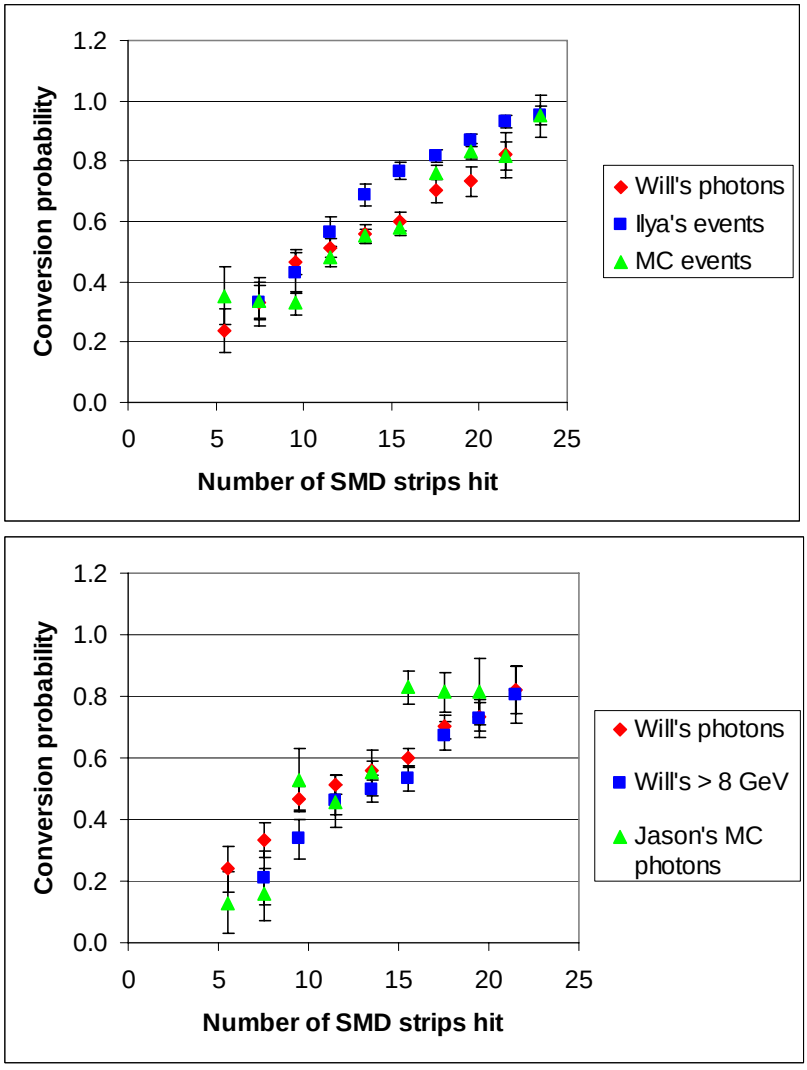

Fig. 18. Conversion probability is plotted as a function of the number of nonzero energy SMD strips. Upper: Will's photon candidates, Ilya's data and Monte Carlo events. Lower: Will's total and >8 GeV photon candidates and Jason's Monte Carlo events.

e. Energy Ratios vs. Number of SMD Strips

Ratios of SMD energy within ±12 strips of the maximum energy strip to the 3 × 3 tower cluster energy were computed as functions of the number of non-zero energy SMD strips for Will's photon candidates, Ilya's data and Monte Carlo events, and Jason's Monte Carlo events. Averages are given in Fig. 19 and two dimensional distributions in Fig. 20 for the case where the pre-shower1 energy was consistent with zero (E_{Pre1}=0). All averages increased with number of strips, with Ilya's data having the smallest ratio, then the two Monte Carlo sets, and finally Will's photons having the largest average for a given number of strips.

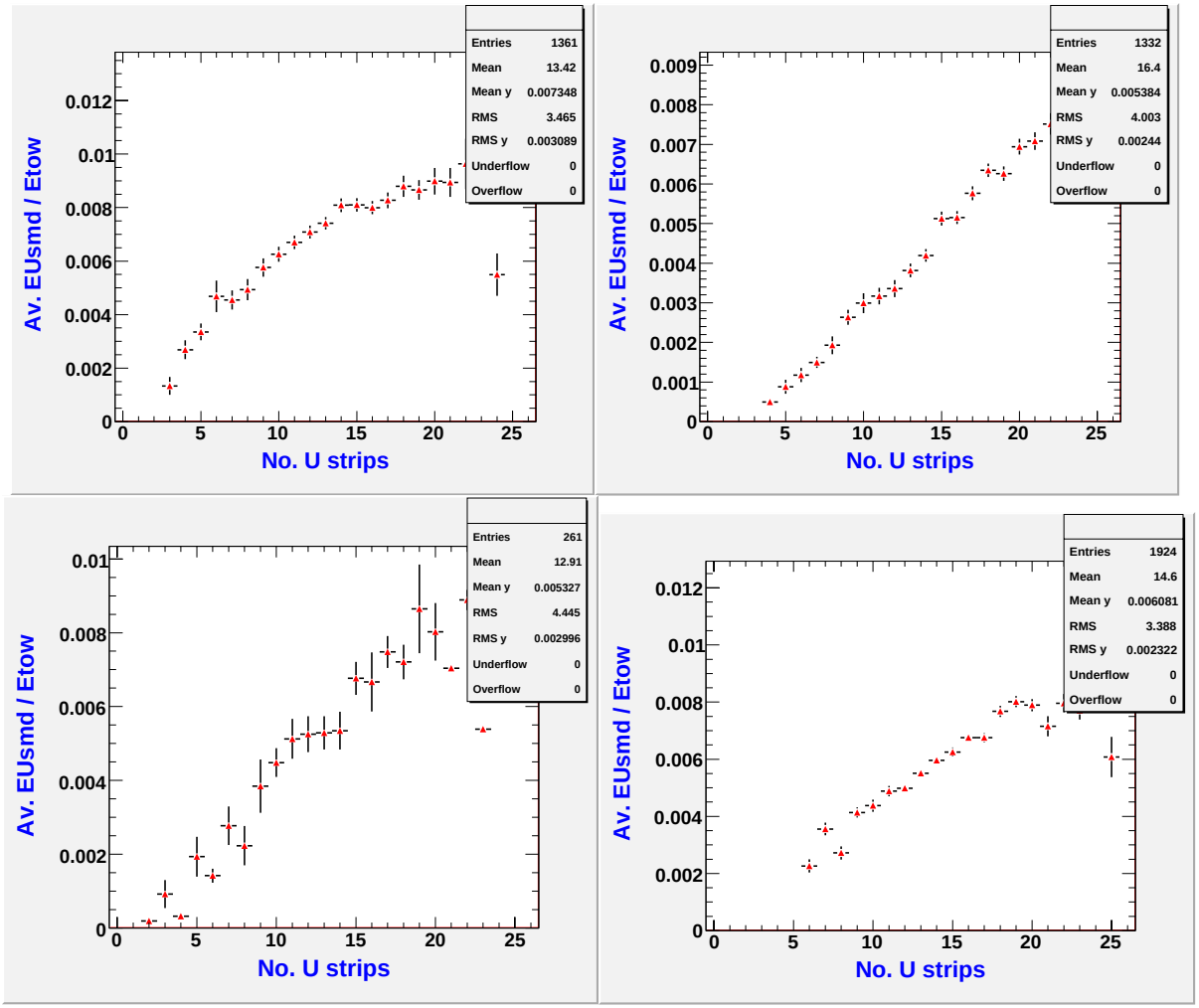

Fig. 19. Average ratios of SMD energy to tower cluster energy as a function of the number of SMD strips with nonzero energy for E_{Pre1} = 0. Upper left: Will's photon candidates, upper right: Ilya's data, lower left: Jason's Monte Carlo events, lower right: Ilya's Monte Carlo events.

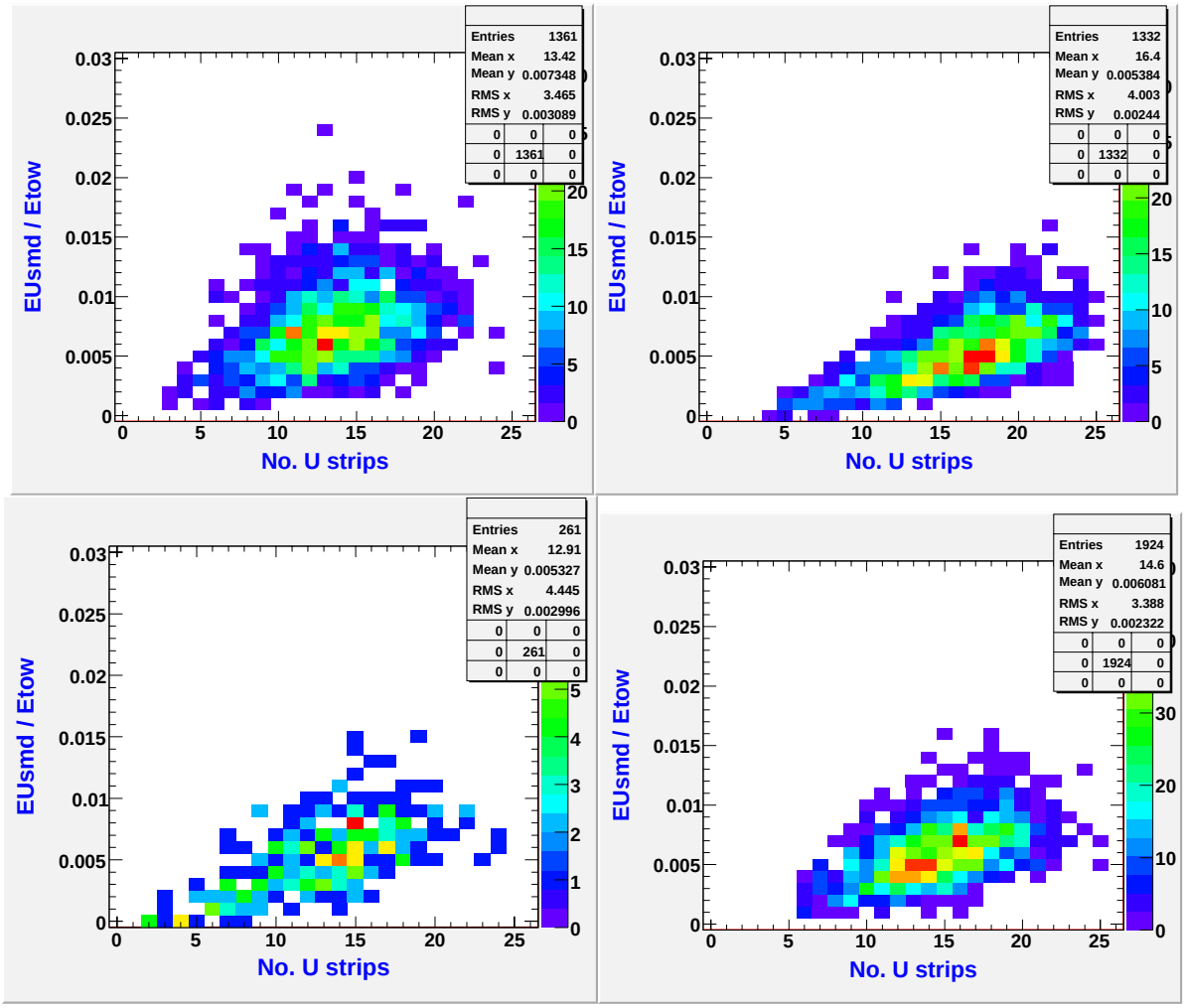

Fig. 20. Two dimensional histograms of SMD energy to tower cluster energy ratio as a function of the number of SMD strips for $E_{Pre1} = 0$. Upper left: Will's candidates, upper right: Ilya's data, lower left: Jason's Monte Carlo events, lower right: Ilya's Monte Carlo events.

Similar plots are given for non-zero pre-shower1 energy in Figs. 21 (averages) and 22 (two dimensional histograms). Only small differences are observed in the averages for the two cases $E_{Pre1} = 0$ and $E_{Pre1} > 0$. As before, Ilya's data had the smallest ratios E_{smd}/E_{tow}, then the Monte Carlo events, and Will's photon candidates had the largest average ratios for a given number of SMD strips with non-zero energy. The two-dimensional distributions for $E_{Pre1} = 0$ look similar, though the peak for Ilya's data occurs at a slightly larger number of strips (~17 vs. ~13-14). However, in Fig. 22 the three $E_{Pre1} > 0$ distribution peaks all seem shifted to the right by 2-4 strips. In particular, Ilya's data peaks ~21 strips, while Will's peaks ~16. It appears that Ilya's data for $E_{Pre1} > 0$ are dominated by events that are somewhat different from Will's photon candidates.

Note in these studies the V strip distributions were also generated and appear identical to those from the U strips. Also, for Ilya's Monte Carlo events, the SMD energy was taken from the simulation, and only the shape from Will's candidate photons.

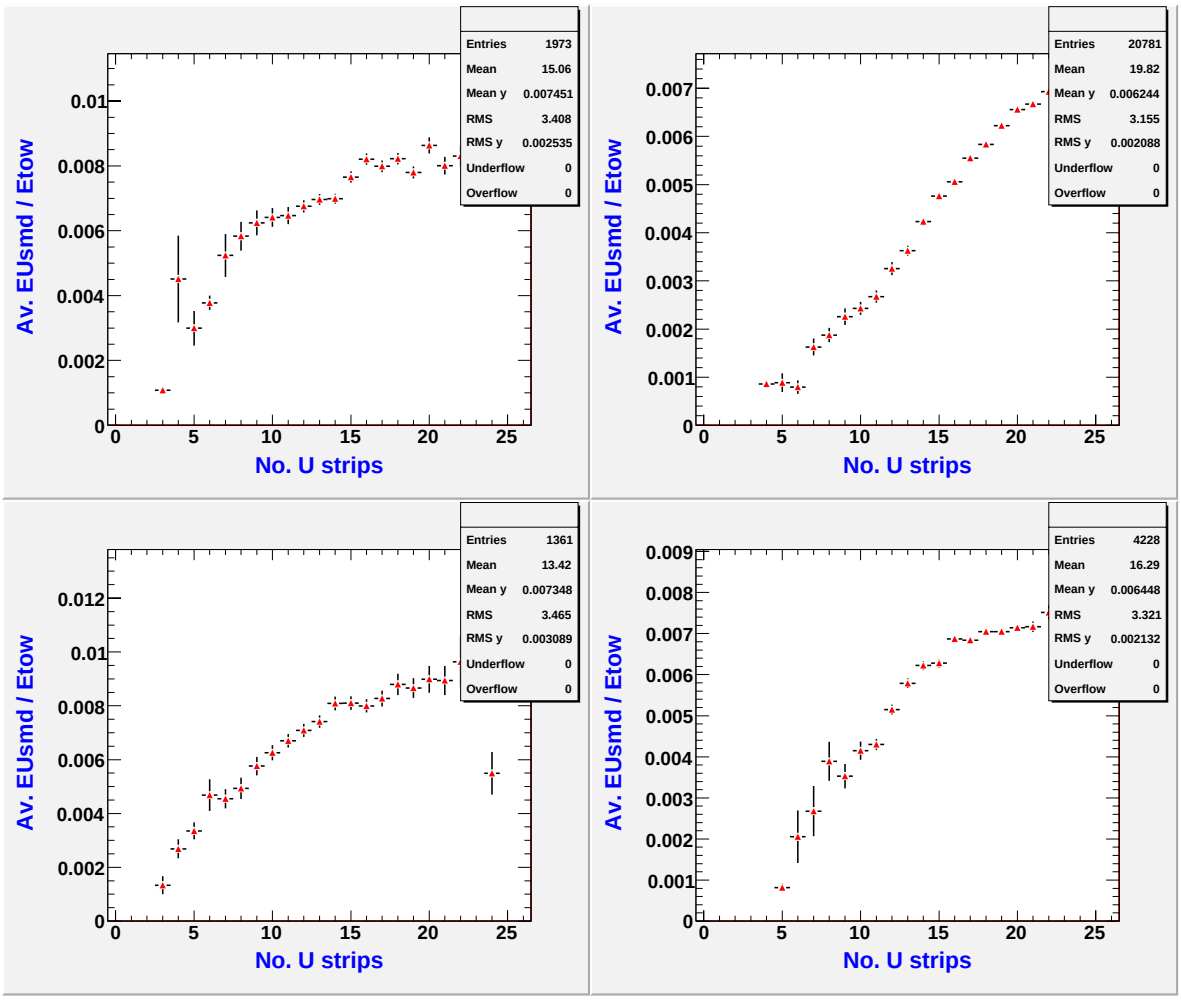

Fig. 21. Average ratios of SMD energy to tower cluster energy as a function of the number of SMD strips with nonzero energy for $E_{Pre1} > 0$. Upper left: Will's photon candidates, upper right: Ilya's data, lower left: Will's events with $E_{Pre1} = 0$, lower right: Ilya's Monte Carlo events.

Another energy ratio was also computed for various data samples, namely the post-shower to 3 × 3 tower cluster energy (E_{post}/E_{tow}). Average values as a function of the number of SMD strips with non-zero energy are plotted in Fig. 23. The ratio from Will's photon candidates is much smaller than from Jason's Monte Carlo events, which in turn is smaller than Ilya's Monte Carlo events. Ilya's data has the largest E_{post}/E_{tow} ratio at all number of strips, and especially at the smaller number of strips.

The reasons for these differences are not clear. The smaller values for Will's photon candidates than for the Monte Carlo predictions may be related to additional material in the actual STAR detector that is not in the simulations. However, this does not explain the differences between the two Monte Carlo predictions. The larger energy ratio for Ilya's events may be related to the presence of hadrons in the event sample, since these would generally shower later in the calorimeter. Note that for these plots there are many

events with the post-shower counter energy consistent with zero. Thus, the two-dimensional plots are not included here.

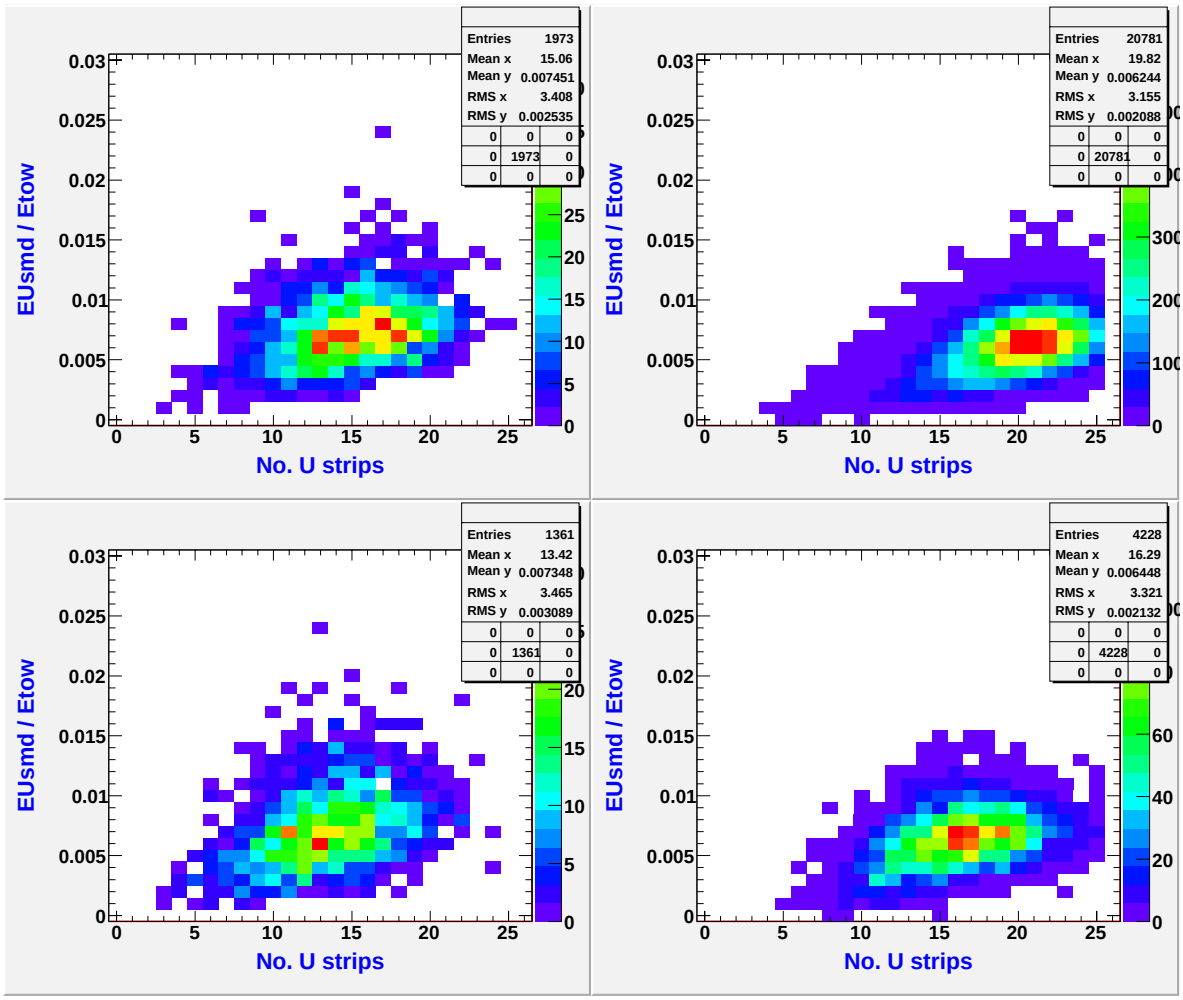

Fig. 22. Two dimensional histograms of SMD energy to tower cluster energy ratio as a function of the number of SMD strips for $E_{Pre1} > 0$. Upper left: Will's candidates, upper right: Ilya's data, lower left: Will's events with $E_{Pre1} = 0$, lower right: Ilya's Monte Carlo events.

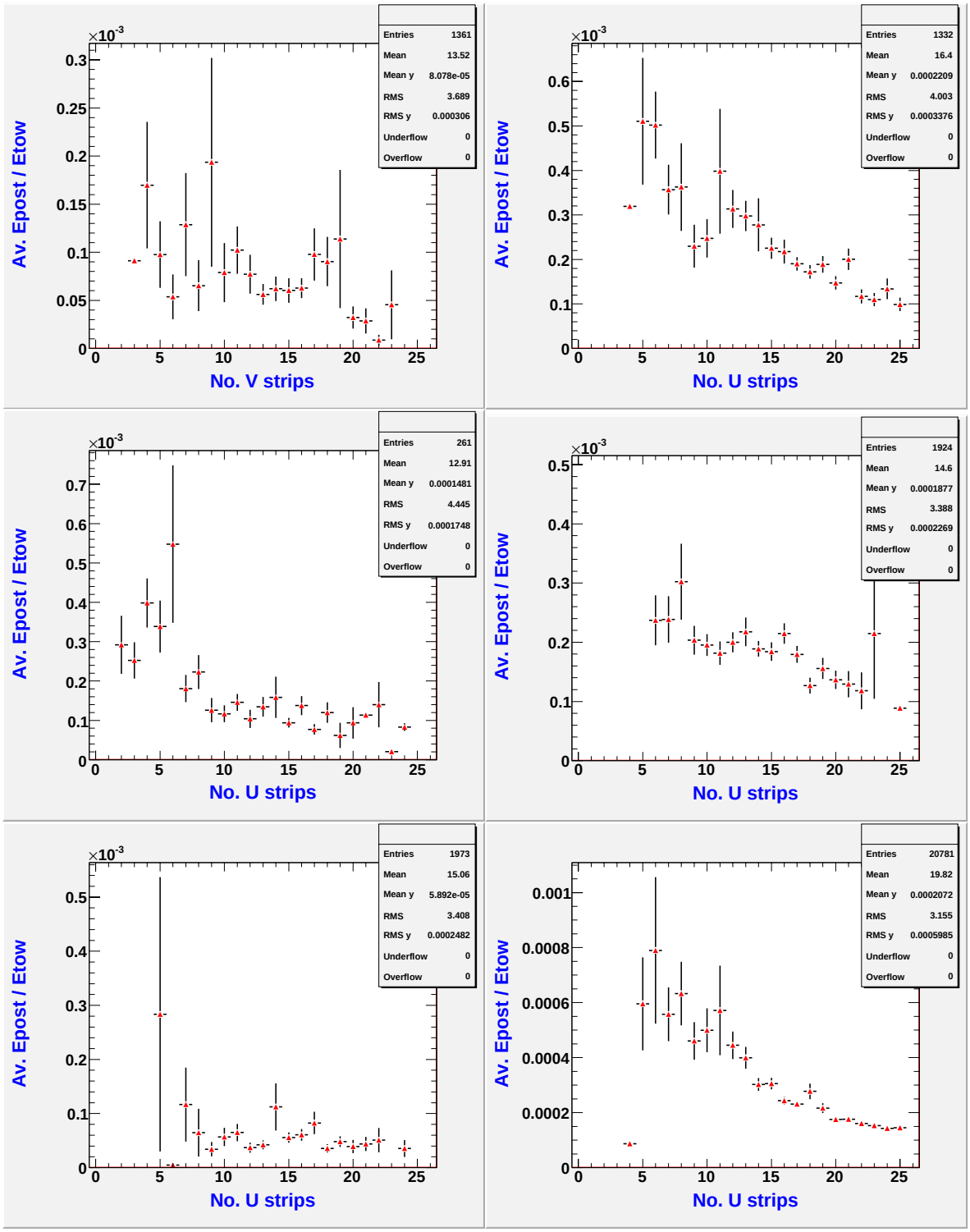

Fig. 23. The average ratio of post-shower to tower cluster energy as a function of the number of SMD strips with nonzero energy is plotted. Upper left: Will's events ($E_{Pre1} = 0$), upper right: Ilya's data ($E_{Pre1} = 0$), middle left: Jason's MC events ($E_{Pre1} = 0$), middle right: Ilya's MC events ($E_{Pre1} = 0$), lower left: Will's events ($E_{Pre1} > 0$), lower right: Ilya's data ($E_{Pre1} > 0$).

f. Chi-Squared Distributions from SMD Shower Shapes

Following the analysis technique described in Refs. 8 and 9 from CDF, a mean shower shape and the associated RMS for each strip was constructed for Will's candidate photons. The mean shape and RMS were used to construct a chi-squared in order to estimate the number of photons in Ilya's data sample.

It was assumed that Will's event sample was mostly photons, although this could not be proved. For example, Fig. 13 indicates a sizeable background under the $\eta \rightarrow \gamma\,\gamma$ invariant mass peak. The composition of the background is uncertain.

At the time of this analysis, Ilya's events were usually separated into four categories based on the energy in the two pre-shower counters: (Pre1=0, Pre2=0), (Pre1=0, Pre2>0), (Pre1>0, Pre2>0), and (Pre1>0, Pre2=0). Will's events were separated into the first three of these four categories, and the shower shapes and RMS values calculated; see Fig. 24. It can be seen that the shapes are quite similar, with the (Pre1=0, Pre2=0) case being slightly narrower and having slightly larger RMS variation in the central three strips.

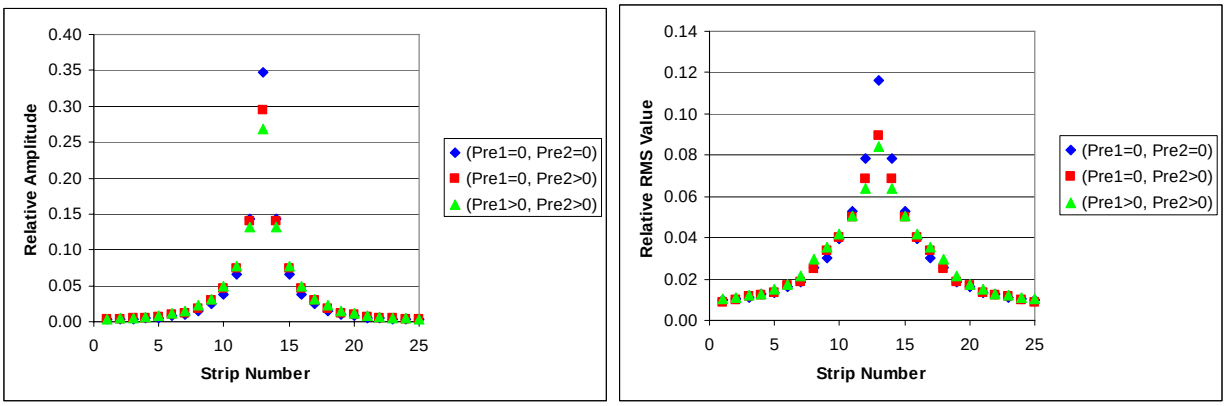

Fig. 24. Comparison of shower shapes and RMS values as a function of SMD strip number for three pre-shower conditions from Will's photon candidates.

The reduced chi-squared for a "photon" was defined to be:

$$\chi^2 = \Sigma\, [\, (\mathrm{Ampl}_i - \mathrm{SS}_i) / \mathrm{RMS}_i]^2 / 50$$

where Ampl_i is the observed photon shower shape (normalized to unit area and centered on the energy weighted mean strip), and SS_i is the shower shape and RMS_i is the associated RMS value from Will's candidate events. The sum is over ±12 strips in both U and V planes of the SMD. A comparison of the chi-squared distributions for Will's ($E > 8$ GeV) and Ilya's events under various pre-shower conditions is given in Figs. 25 and 26.

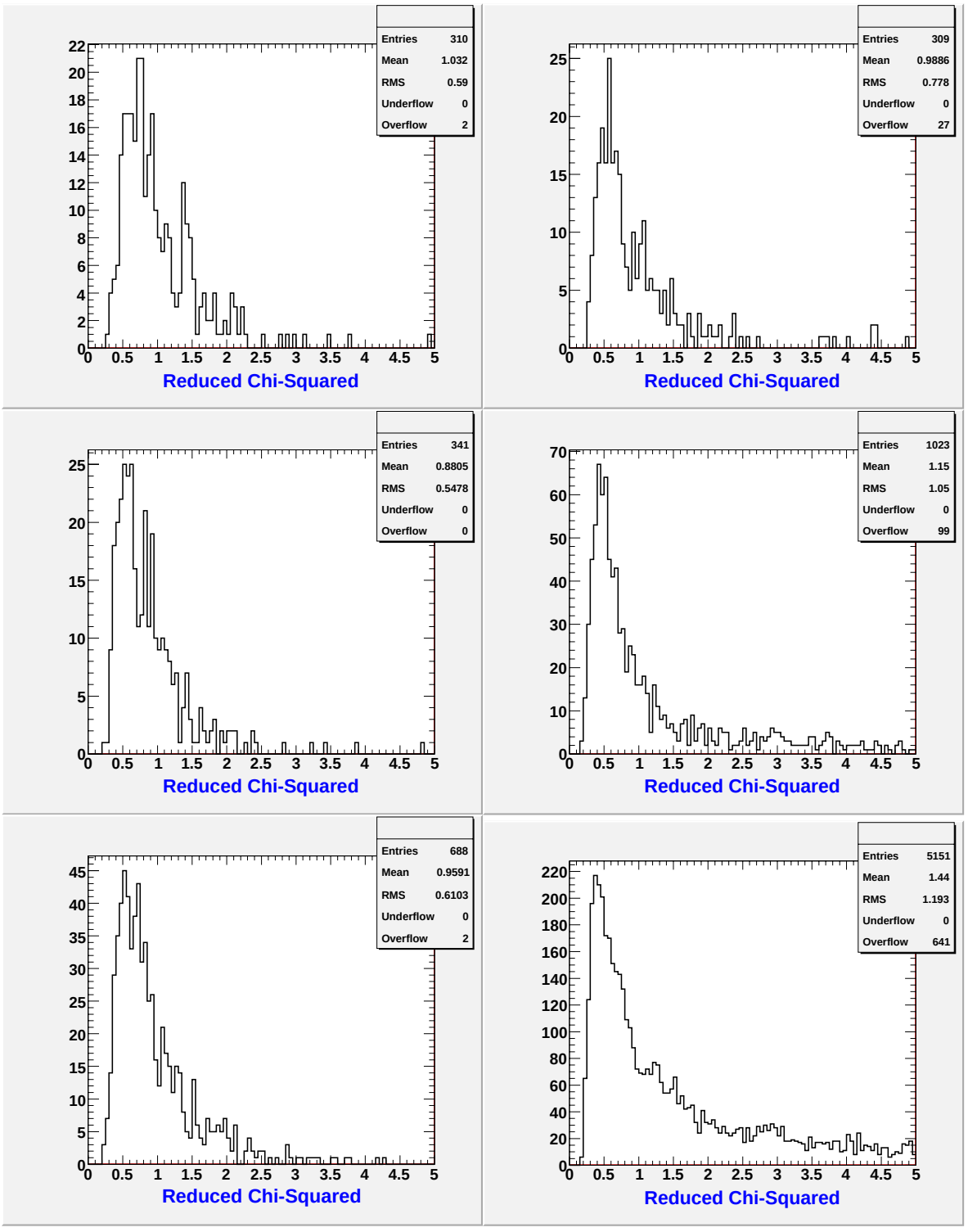

Fig. 25. Chi-squared distributions for Will's photon candidates (left) and Ilya's events (right). The upper plots correspond to ($E_{Pre1} = 0$, $E_{Pre2} = 0$), the middle ones to ($E_{Pre1} = 0$, $E_{Pre2} > 0$), and the bottom ones to ($0 < E_{Pre1} < 5$ MeV, $E_{Pre2} > 0$).

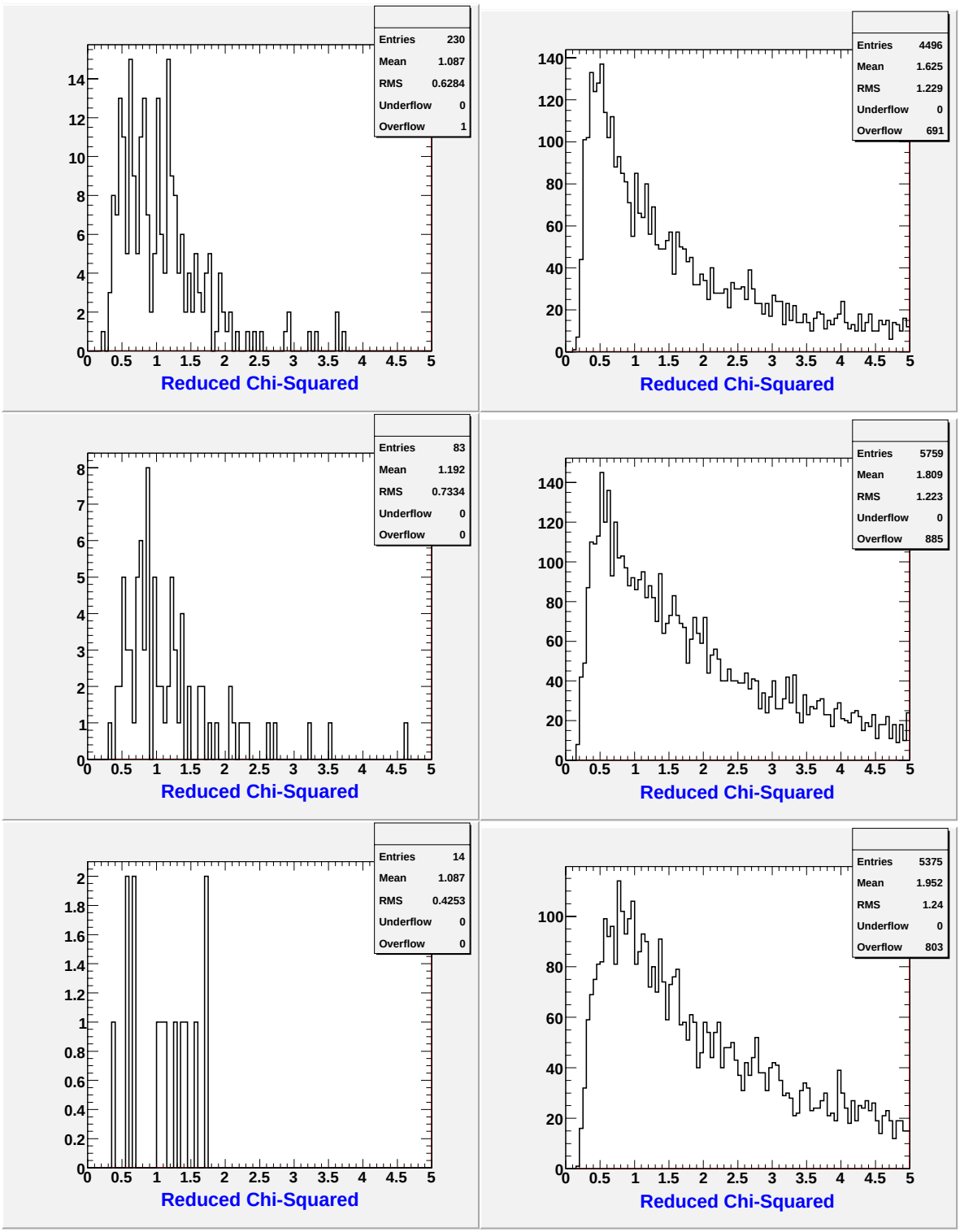

Fig 26. Chi-squared distributions for Will's photon candidates (left) and Ilya's events (right). The upper plots correspond to ($5 < E_{Pre1} < 10$ MeV, $E_{Pre2} > 0$), the middle ones to ($10 < E_{Pre1} < 20$ MeV, $E_{Pre2} > 0$), and the bottom ones to ($E_{Pre1} > 20$ MeV, $E_{Pre2} > 0$).

The reduced chi-squared distributions for Will's photon candidates are quite similar for all six conditions in Figs. 25 and 26, though some minor differences are probably present and the statistics for one case is very poor. All have mean values near 1.0 and RMS widths approximately 0.6. (This is the justification for using all of Will's sample with E > 8 GeV for constructing the shower shape, independent of pre-shower counter energy conditions.) On the other hand, significant changes are observed in the distributions for Ilya's events. Thus, although the three pre-shower conditions in Fig. 25 suggest that Ilya's data contain a good fraction of events that have shapes similar to Will's photon candidates with E > 8 GeV, the fraction of such events is quite small in the three cases in Fig. 26. Note this is consistent with the qualitative results reported in Sec. 2 looking at individual events "by hand."

It was attempted to estimate the number of photons in Ilya's events using the chi-squared distributions and information from Refs. 8 and 9 for background shapes. Very generous uncertainty estimates were assumed. Only events with reduced chi-squared values between 0 and 0.9 were included. The background estimates for the cases (E_{Pre1}=0, E_{Pre2}=0), (E_{Pre1}=0, E_{Pre2}>0), (0<E_{Pre1}<5 MeV, E_{Pre2}>0), and (5<E_{Pre1}<10 MeV, E_{Pre2}>0) were (4 ± 2)*12 bins, (12.5 ± 6)*12 bins, (55 ± 20)*13 bins, and (60 ± 20)*13 bins, respectively. This gave an estimated number of photons in the four cases of (122 ± 27), (417 ± 76), (1428 ± 264), and (671 ± 263), and signal to background ratios in the reduced chi-squared peak were about 2.5, 2.8, 2.0, and 0.9, respectively. The total number of "photons" is very approximately 2640 ± 380, where it is assumed that there are few photons in the last two cases in Fig. 26 and these would be extremely difficult to extract given the very poor signal to noise. Obviously, this analysis needs to be repeated with real estimates of background shapes from simulations and data. However, it is clear that it will be quite difficult to extract a good photon signal from Ilya's data when there is more than 5 – 10 MeV present in the pre-shower1 counters corresponding to the photon candidate 3 × 3 tower cluster.

g. Left-Right Shower Shape Differences

As described in Sec. 3.c, shower shapes for Will's candidate photons were obtained for all energies (3334 events) and for those with E > 12 GeV (574 events). The area for each event was normalized to unity, and the center placed at the energy weighted mean strip. The shapes were summed for all events, so that their areas were 3334 and 574, respectively. Left (smaller strip number) – right differences about the center were computed, and the results shown in Fig. 27, where the 5 central strips are omitted. At small distances from the center, the differences are positive, while at larger distances they are negative. The shapes seem different for the two cases as well.

Left-right asymmetries were formed by summing all counts in the shower shapes for 3 or more strips from the center. The asymmetries were +0.0034 and +0.0004 for the U and V SMD planes for all events, while the asymmetries were -0.0016 and -0.0023 for U and V, respectively for E > 12 GeV candidates. (It is presently unclear how to estimate statistical uncertainties on these values or the entries in Fig. 27.)

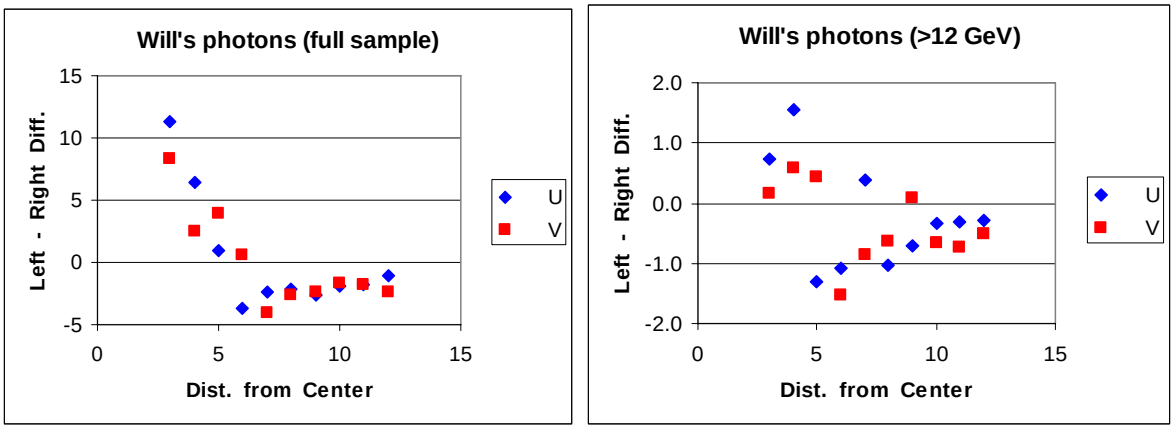

Fig. 27. Left-right shower shape differences for Will's photon candidates are plotted as a function of distance from the center of the shower (in strips). The results for the full sample of 3334 events is shown on the left, while the sample with energy larger than 12 GeV (574 events) is shown on the right.

One contribution to the left-right differences may be the varying lengths of SMD strips, due to the fact that the strips are at a 45º angle to the SMD symmetry axis. The strip lengths first increase, and then decrease in length with increasing strip number. In order to test whether this might be (one of) the explanation(s) for the observed asymmetry, the data were subdivided by pseudo-rapidity and differences computed as before. The results are shown in Fig. 28. Differences in the three cases are apparent. For pseudo-rapidity = 1.0 – 1.4, the number of events was 1439 and the U and V plane asymmetries were +0.0151 and +0.0119, respectively. For $\eta = 1.4 - 1.6$, there were 1153 events and the asymmetries were +0.0096 and +0.0102, and for $\eta = 1.6 - 2.0$, there were 675 events with asymmetries -0.0358 and -0.0425.

Even though the shapes of the difference distributions and the signs of the asymmetries changed as a function of pseudo-rapidity, it is not clear that the changing SMD strip lengths are solely responsible for the observations. For example, all distributions in Figs. 27 and 28 have negative differences at larger distances from the center of the "photon", whereas it would have been expected to change sign for regions where the strip length was increasing versus where it was decreasing.

Finally, when computing the reduced chi-squared or other shower shape dependent quantities, the left-right differences may need to be taken into account to accurately derive results of interest.

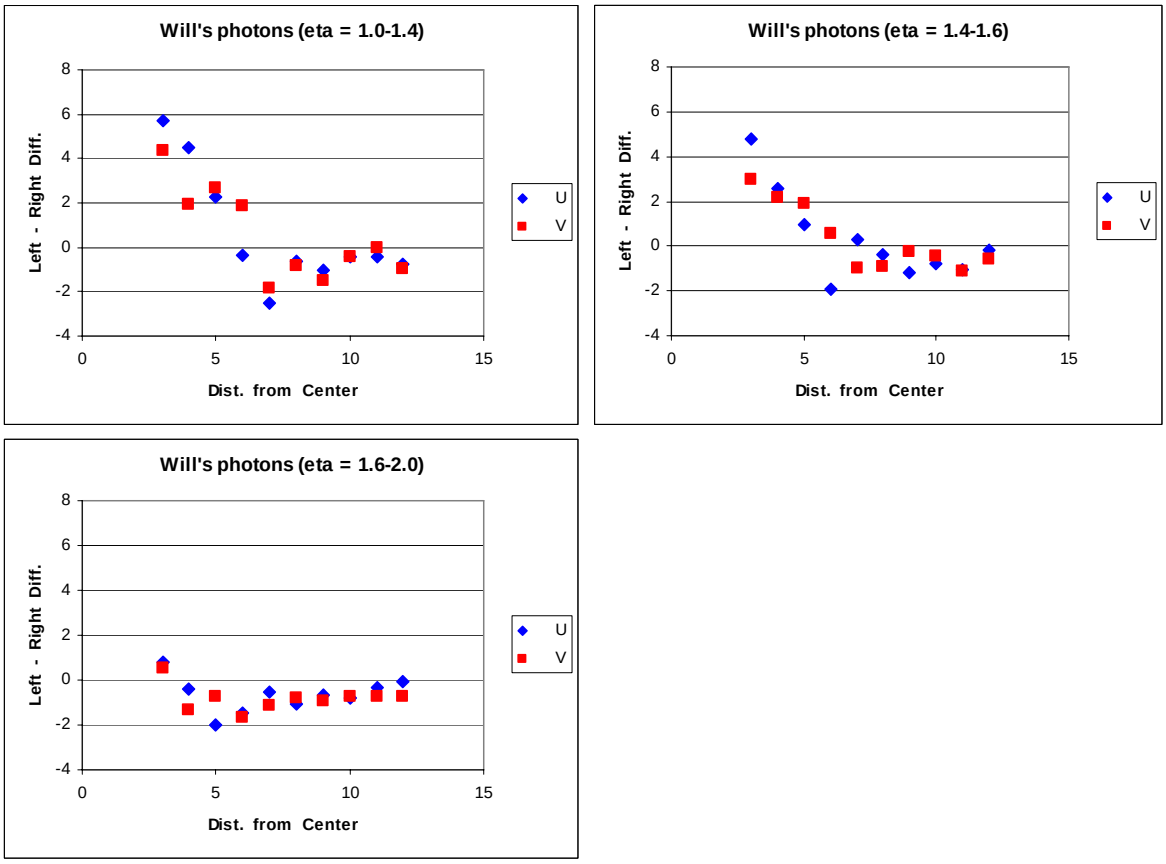

Fig. 28. Left-right shower shape differences for Will's photon candidates are plotted as a function of distance from the center of the shower (in strips). No energy cut is applied to the data, and three different pseudo-rapidity (eta) ranges are plotted.

4. "x-ray" STAR

The material in front of the EEMC was effectively "x-rayed" using Will's photon candidates. This was done by comparing the number of events with the pre-shower1 energy = 0 (no charged particles) to the number of events with the pre-shower1 energy >0 (events with gamma conversions). Note that averaged over the EEMC, about 60 percent of gammas from etas do convert before the endcap pre-shower1 counters, so about 40% do not convert; see Sec. 3.d. This analysis has been limited by four factors:

- The statistics are limited. This was partially overcome by grouping of 3 x 3 SMD patch (cluster) information and by reflections about the phi center of a sector, at the expense of spatial resolution.
- We don't know what fraction of events might actually have two gammas within a 3 x 3 patch, although there are strong indications that it is not very much.
- In the "canned" root Ntuple sample of gammas from etas, we do not have the flexibility to vary some parameters, such as patch size. In practice, we would

want to go to smaller patches, but don't have the statistics even for the existing 3 x 3 patches, so this is not a practical limitation when using all the etas which were reasonably extracted from the 2006 data within the constrains of having both gammas within one sector.

- We have little knowledge of the mass of the silicon SVT and SSD detectors near the vertex or the associated supports and cabling. Also we do not know the extent to which gamma conversions in this material near the vertex are swept out by the magnetic field before reaching the EEMC.

There are many subtleties to this kind of analysis. First of all, the distribution pattern of gammas over the endcap calorimeter is not used in the calculation, only ratios. If we were using direct photons to x-ray the EEMC, it would be fairly straightforward. However, in fact a lot of the time the large area 3 x 3 tower-cluster-size pre-shower1 patch catches either the gammas or the conversion products from both gammas in an η decay. To handle this feature really correctly, the number of gammas in a 3 x 3 patch would need to be known. In most of this analysis we assume it is one, although we should in fact Monte Carlo both the acceptance for two gammas from each η as a function of position, and also the other π^0's, etc. in the general direction of an η in each event. There is some crude information on this issue later in this section.

It can be seen that there are more gammas from $\eta \rightarrow \gamma\,\gamma$ decays found near the edges of sectors than in the middle of sectors; see Figs.29 and 30. This could be due to the need to find the second gamma in the same EEMC sector in the present version of the software. Another interesting aspect is that the kinematics of separation between two gammas in an η or π^0 decay is not so far from the minimum opening angle, even for rather large ratios of the gamma energies.

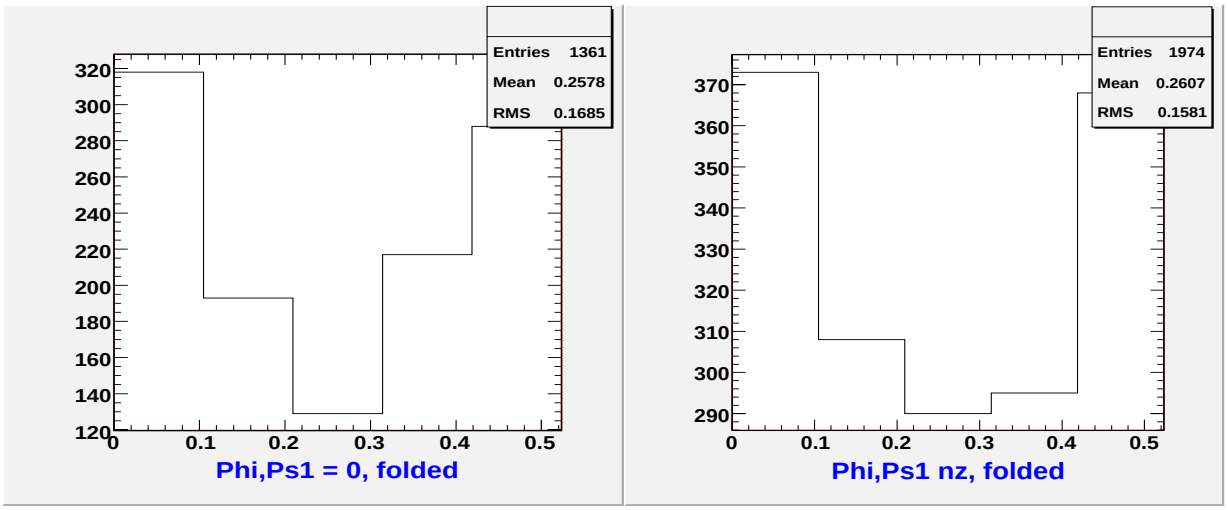

Fig. 29. The number of events vs. phi folded to the width of 1 sector is plotted. Events with $E_{Pre1} = 0$ are on the left and $E_{Pre1} > 0$ are on the right.

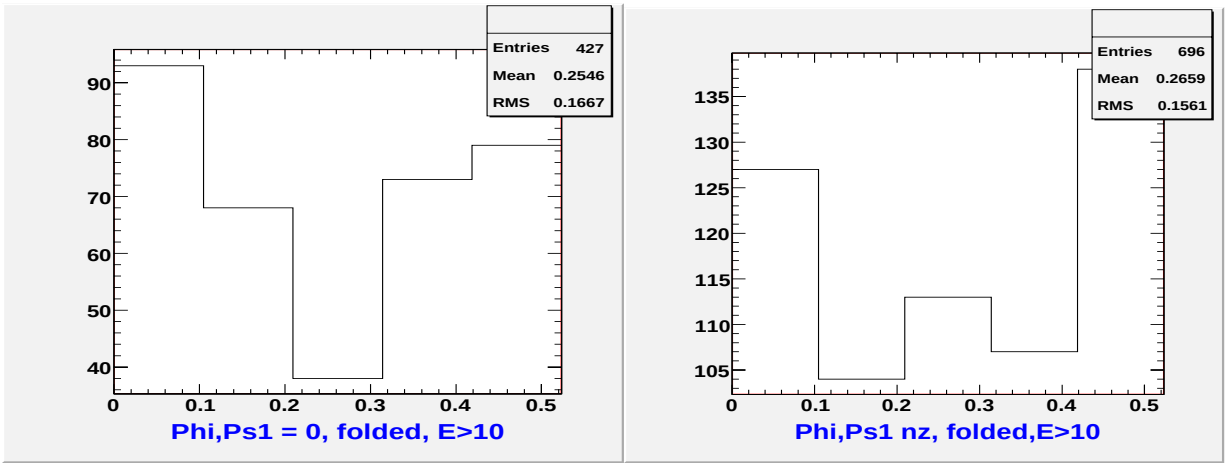

Fig. 30. A subset of the data in Fig. 29 is shown, with a cut requiring $E_{tower} > 10$ GeV.

Plotting the number of photons with $E_{Pre1} = 0$ vs. phi over the EEMC showed a regular structure, which could be due to the constraint that both gammas of an eta be within one sector. The two gamma separation is of the same order of the sector size, so one will generally be near an edge since the finder does not cross sector boundaries. However, by comparing the number with $E_{Pre1} = 0$ vs. $E_{Pre1} > 0$, we should be able to find the number of radiation lengths in front of the EEMC vs. position. First, consider just two positions - center and edges of a sector.

The number of gammas surviving the material in front of the EEMC is

$$N = N_0 \exp[-x / (9\ X_0/7)] ,$$

where N_0 = the original number of gammas
x = the distance the gamma traveled in radiation lengths
X_0 = the radiation length of the material along the path of the gamma.

The probability that a single gamma survives is

$$P1 = N / N_0 = \exp [-x / (9\ X_0 / 7)].$$

This probability can be calculated from data by comparing the events with and without energy in the pre-shower1 counter.

$$P1 = \#(E_{Pre1} = 0) / [\#(E_{Pre1} = 0) + \#(E_{Pre1} > 0)].$$

So for example from Fig. 29, P1 =1361 / (1361 + 1974) = 0.408. This gives $x / X_0 = 1.15$, which is averaged over the endcap because Fig. 29 is all sectors folded together. The big variations with phi may be due to the TPC vanes. Looking at different values of phi, we get for phi = 0, $x / X_0 = 1.03$ and for phi = 0.2618, $x / X_0 = 1.52$, indicating more material

at this angle. Using Fig. 30, which has a cut on $E_{tower} > 10$ GeV, we get $x / X_0 = 1.19$ at phi = 0 and $x / X_0 = 1.73$ at phi = 0.2618, but with larger statistical errors of at least 10%.

Figure 31 shows a plot of the radiation length of material vs. pseudo-rapidity just from the aluminum TPC wheel, without electronics or cooling water pipes.

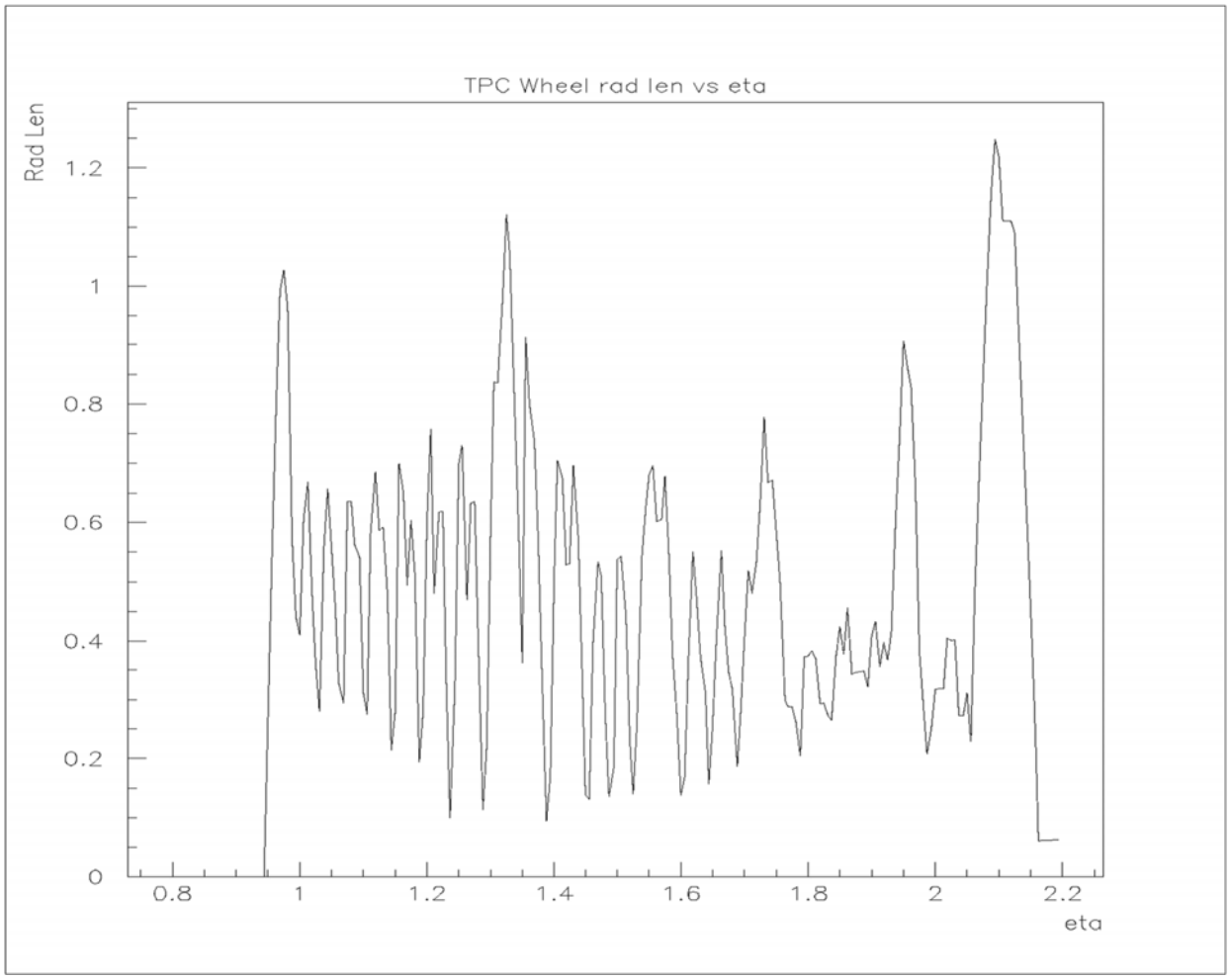

Fig. 31. The expected variation in radiation lengths versus eta (pseudo-rapidity) in the EEMC for the TPC wheel only.

Figure 32 contains a diagram of the estimated material at the end of the TPC included in simulations. This includes electronics, G-10 boards, water pipes, and support structures. We do not have a clear plot of the radiation lengths vs. position for this configuration (because Star simulation code was changed).

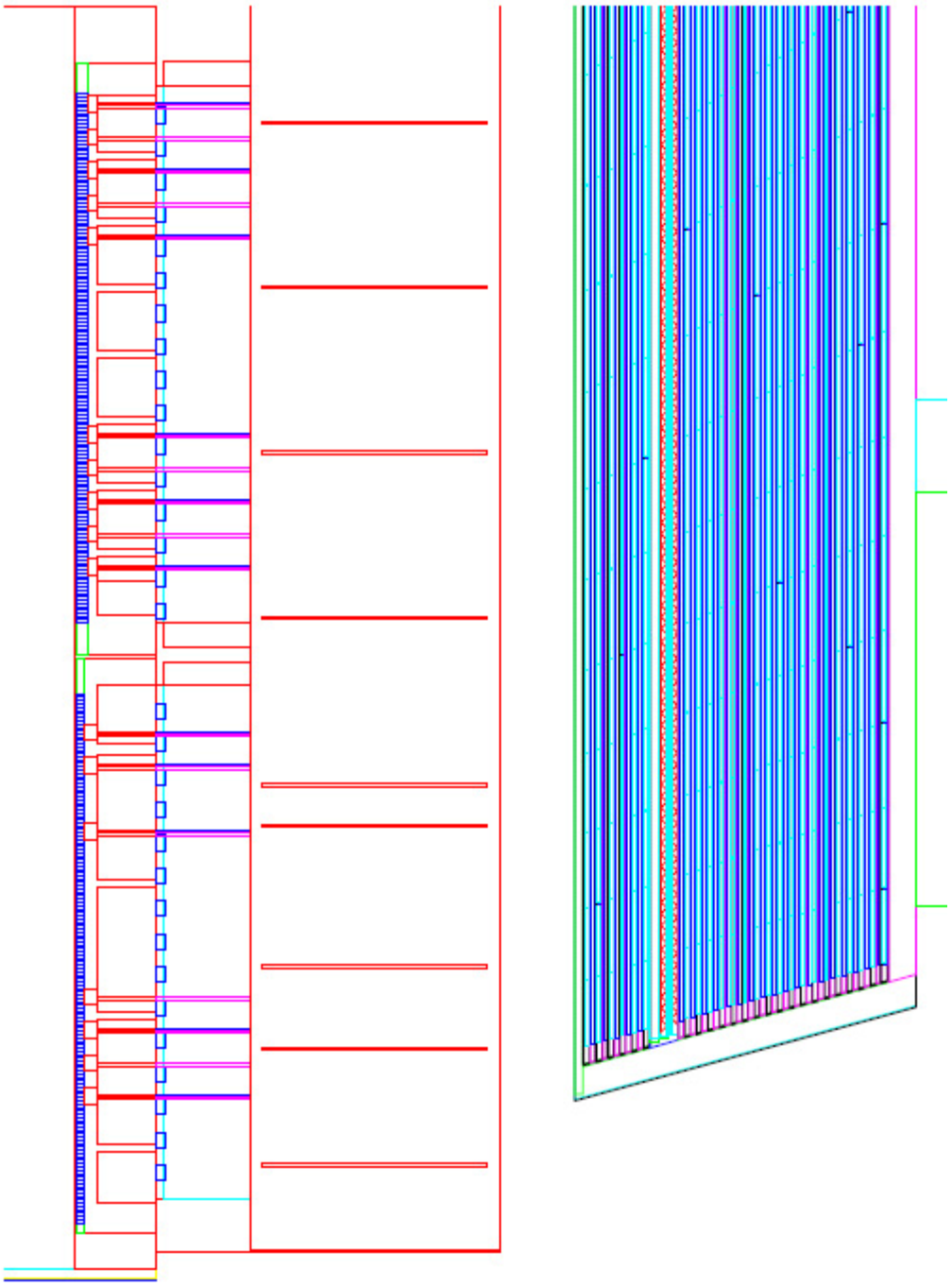

Fig. 32. The material which was entered into GEANT is shown, including aluminum TPC wheel, water pipes, aluminum bars to clamp FEE (front end electronics) cards, hundreds of small G-10 boards for FEE, large G-10 boards, etc.

If we assume two photons, then the probability of no gamma conversion is P(no conversion) = (P1)*(P2) = $(P1)^2$, assuming the probabilities are the same, so the probability of at least one gamma conversion is 1 – $(P1)^2$. Note P1 = (1 – Conv. Prob.) defined previously.

Originally, we looked at plots vs. pseudo-rapidity of the number of events with E_{Pre1} = 0 or > 0 and they do not show any significant structure, probably because the interaction vertex was implicitly at z= 0, but in reality has a large range, with rms of 60 cm. Thus any structure between the vertex and the EEMC SMD would get washed out in a plot of events as a function of eta.

This was corrected in later attempts as follows: The hit of the photon was found in the SMD in the transformed X-Y coordinates, where Y is along the eta (pseudo-rapidity) direction. Next, the physics eta and the distance to the SMD were used to find the Z of the vertex. Then the actual photon path could be used to find the intercept with e.g. the TPC wheel, for plotting radiation length vs. position. We can plot vs. position near the TPC and EEMC, by using the shower centers at the SMD. This shows some structure, but the statistics are not so good in fine bins, only ±10 % of a radiation length (see Fig. 33 below). Figures 34 and 35 give one dimensional projections of the events on the x and y directions.

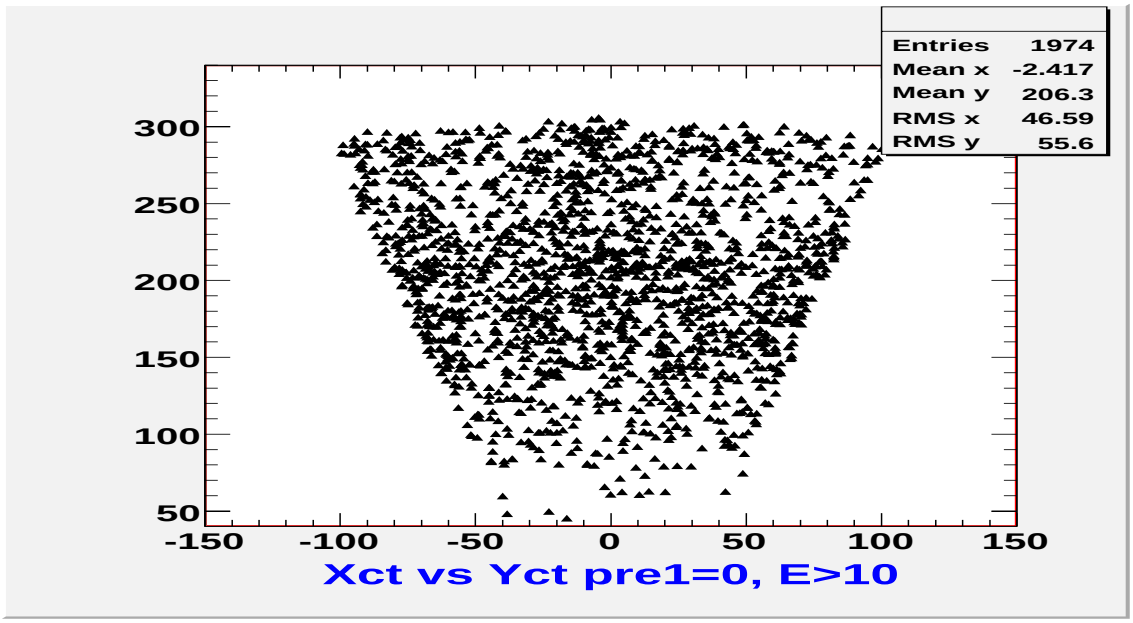

Fig. 33. The number of events in the SMD converted to x-y coordinates.

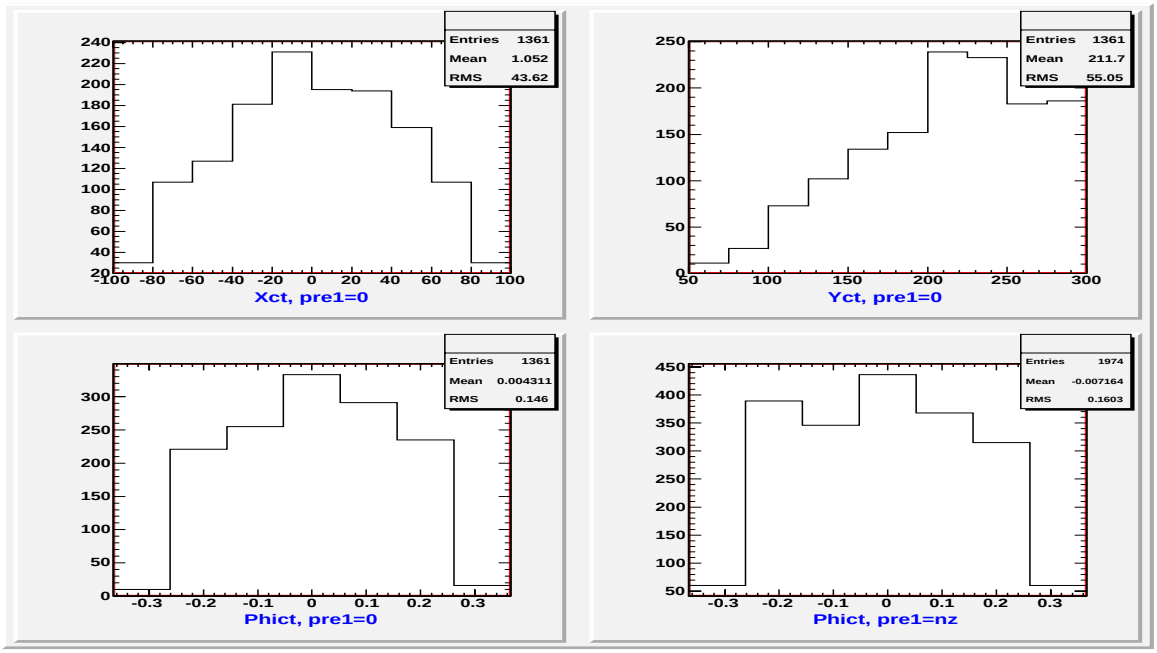

Fig. 34. x and y plots requiring the energy in the pre-shower1 counter to be = 0. The bottom two plots are the number of events vs. phi for $E_{Pre1} = 0$ and $E_{Pre1} > 0$.

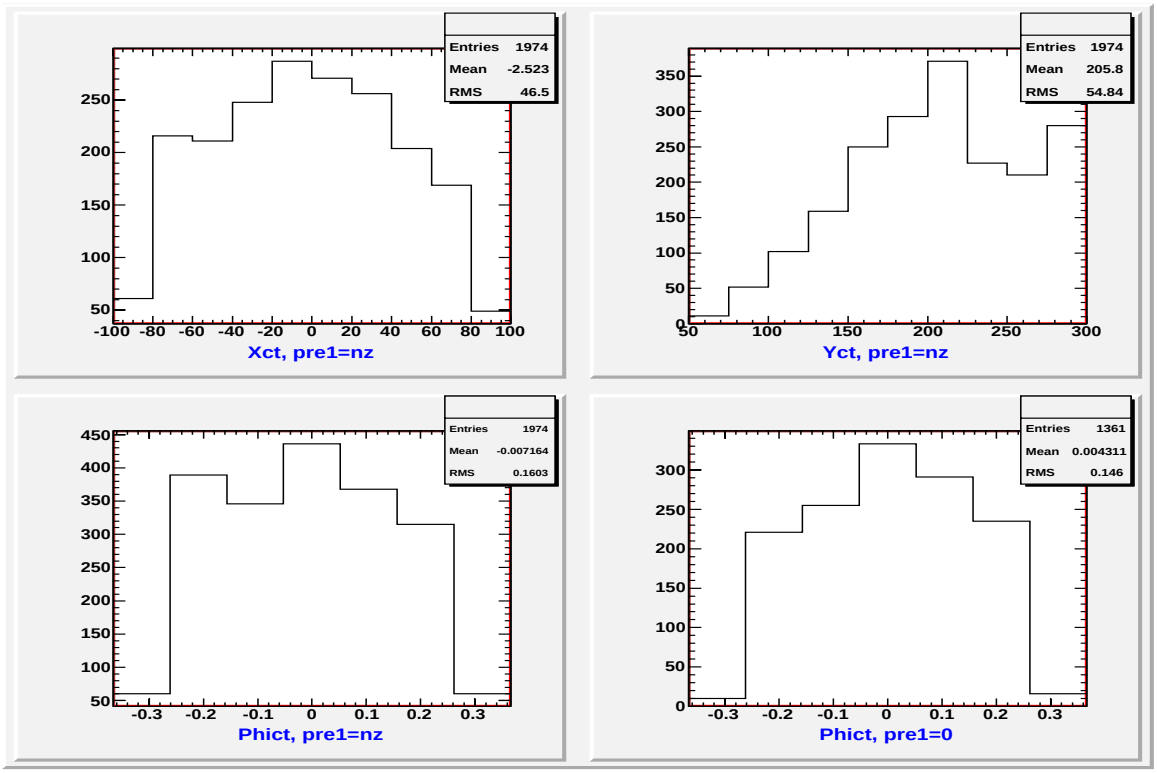

Fig. 35. On top are x and y plots requiring the energy in the pre-shower1 counter to be >0. The bottom plots duplicate the bottom of Fig. 33 above.

In order to more effectively look for structure with limited statistics, The data were re-plotted in a coordinate system aligned with known structures in the TPC wheel and TPC electronics, namely with x perpendicular to R at the center of a sector. A plot vs. Y might then show bands at known structures. Phi was then recalculated as a cross check after using the poorly known offset in Y from the beam axis. The change of coordinates was made by the following coordinate conversion equations:

```
  Xct = 0.5*(.707*Uct - .707 *Vct);
  Yct = 0.5*(.707*Vct + .707*Uct);
 Ypct = Yct +41.0;
  Rct = sqrt(Xct*Xct +Ypct*Ypct);
Phict = atan(Xct/Ypct);
Theta = 2.0*atan(exp(-eta)).
```

Sectors 3 and 9, which overlap with the TPC mechanical supports, were separated out in the analysis, while the remaining sectors were summed. Again, the fraction of "photons" converting before the pre-shower1 counter was used to estimate the amount of material, x / X_0. As Scott Wissink has pointed out (Ref. 7), this method is less sensitive to gamma conversions near the interaction vertex than to conversions near the end of the TPC, due to the STAR magnetic field separating the $e^+ + e^-$ pairs from a conversion. Referring to Fig. 36, there appears to be less material near Y = 240 cm and near phi = 0

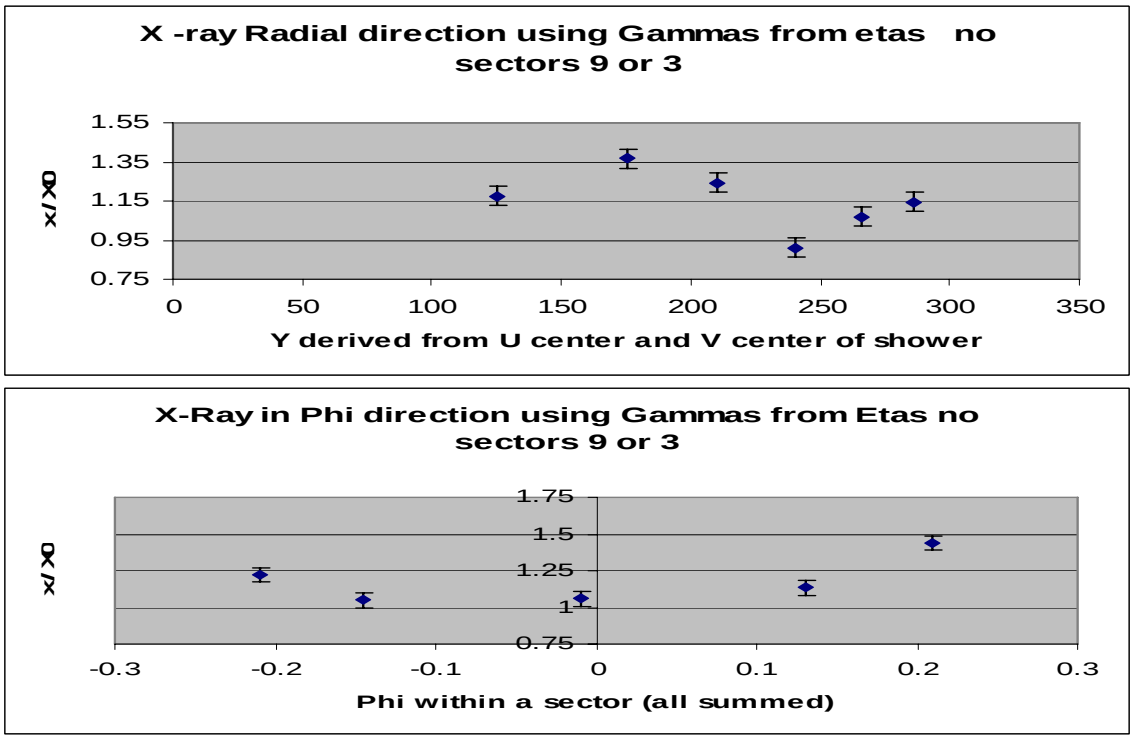

Fig. 36. The derived amount of material, x / X_0, is plotted as a function of the radial coordinate Y (upper) and phi (lower) within a sector; see the text for details.

than near the edges of a sector. Figures 37 and 38 were used to generate Fig. 36, and in Fig. 37 the plots for sectors 3 and 9 seem to be uneven compared to the other sectors, perhaps as a result of the TPC supports.

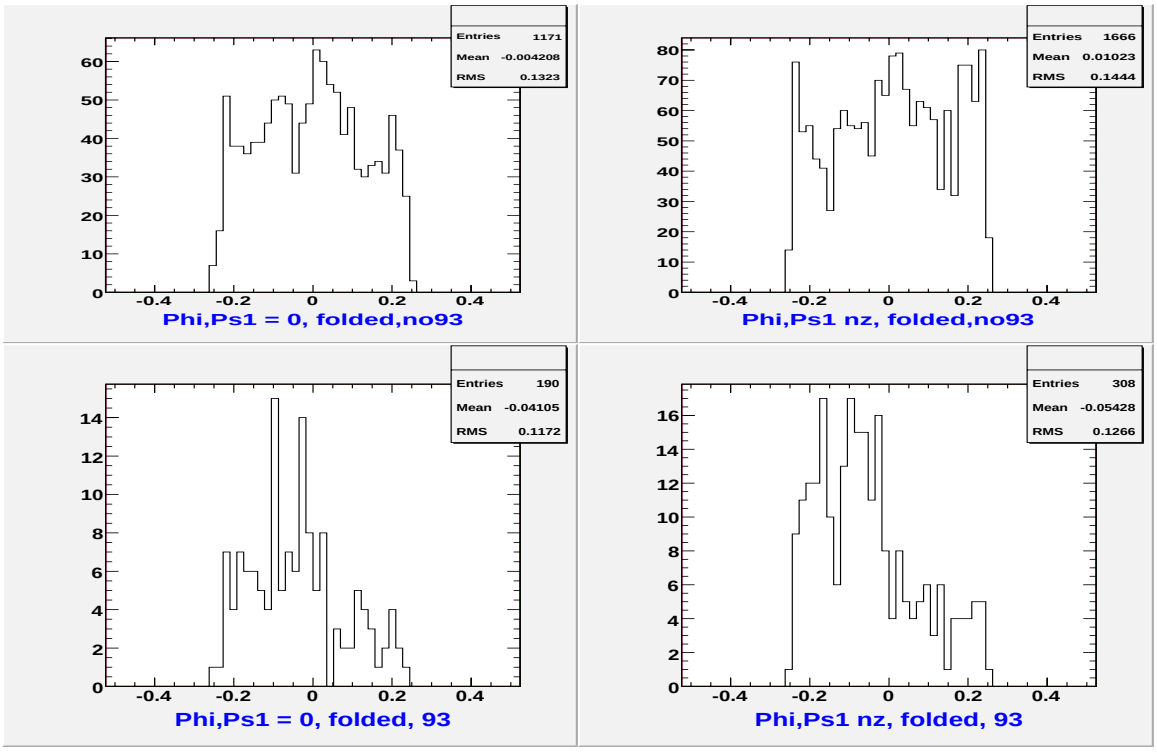

Fif. 37. The number of Will's photon candidates as a function of phi is plotted, "folding" the results so the center of all sectors corresponds to φ = 0. Upper: all sectors except 3 and 9, Lower: sectors 3 and 9, Left: events with $E_{Pre1} = 0$, and Right: events with $E_{Pre1} > 0$.

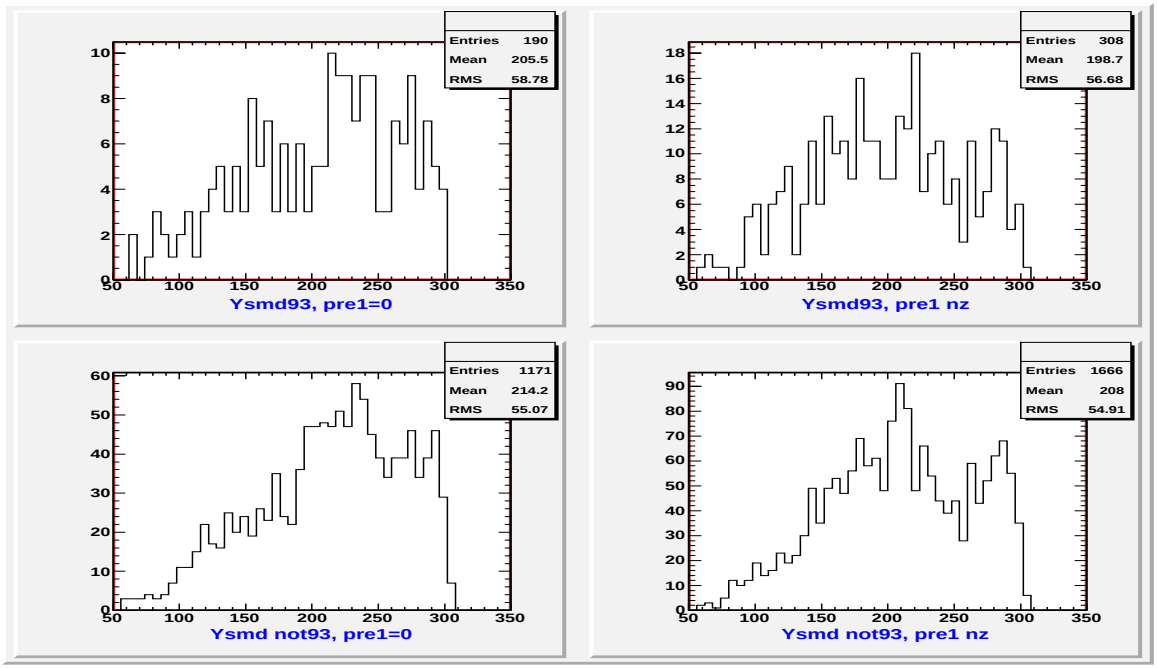

Fig. 38. The number of Will's photon candidates as a function of Y, defined in the text. Upper: sectors 3 and 9, Lower: all sectors except 3 and 9, Left: events with $E_{Pre1} = 0$, and Right: events with $E_{Pre1} > 0$.

In Fig. 39 is displayed the amount of material, in radiation lengths, as a function of pseudo-rapidity for two new, and very large, detectors at the Large Hadron Collider at CERN (see Ref. 10). Note that the material is significant in the region near $\eta \sim 1.5$, just as it is for STAR, and of comparable magnitude as well. Great care must be exercised in the detector design in order to keep the amount of material small.

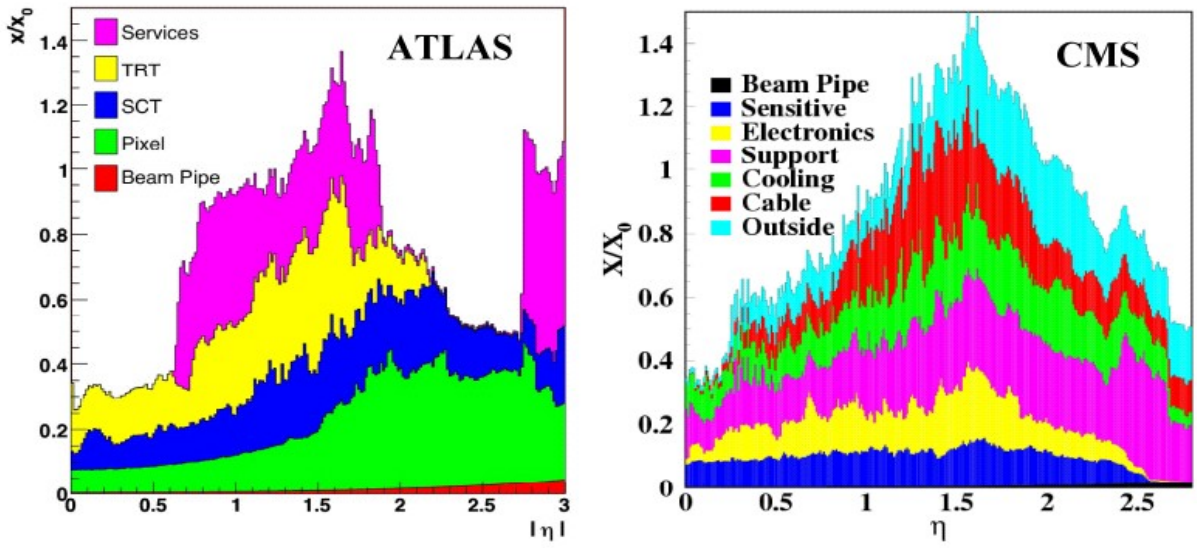

Fig. 39. Different sources of ATLAS/CMS material from Ref. 10.

There is a concern that the amount of material derived from these x-ray studies is considerably beyond what is in simulation models of the STAR detector. For example, the minimum derived thickness in Fig. 36 is about 0.8 X_0 and the maximum is roughly 1.5 X_0; the expected values are considerably smaller. One possibility is that multiple photons are present within the 3 × 3 pre-shower cluster. Note that the calculated number of radiation lengths would decrease by a factor of 2.0 for 2 photons per cluster compared to one photon per cluster.

The results from Will's photon candidates were subdivided into four energy bins as shown in Fig. 40. The largest derived amounts of material are observed from the lowest energy photons, perhaps suggesting that these frequently have more than one photon in the cluster, but there may be only one photon at higher energies.

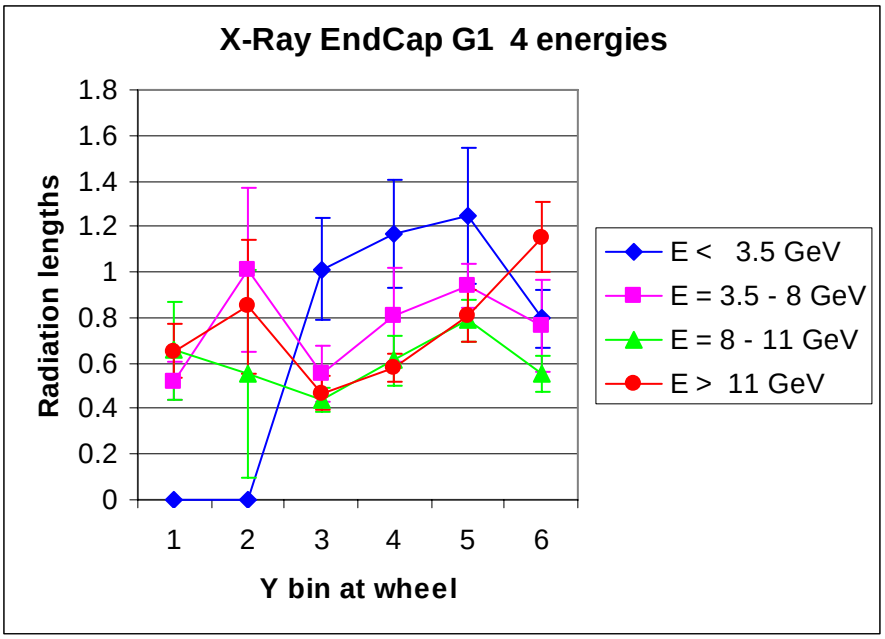

Fig. 40. The derived amount of material in radiation lengths is plotted as a function of radial coordinate Y for four photon candidate energies. One photon per cluster is assumed. Note that the Y bins are not uniform, but were selected to get roughly equal statistics. In particular, bin 2 is a factor of 4 narrower than some others, and is near the projection of the aluminum vane in the TPC wheel.

5. Shower characteristics for events with charged particles

In order to study events with charged tracks, a different sample of events from Pibero (Ref. 11) was used. These events required a tower with the highest transverse momentum (seed tower) to have $P_T > 1.5$ GeV/c, and $P_T > 0.5$ GeV/c for additional towers to be included in the 3 × 3 cluster centered on the seed tower. The photon candidate (sum of the 3 × 3 towers) was required to have $P_T > 5$ GeV/c. Information for any SMD strip within ±20 cm of the center of the seed tower and for any TPC track within a radius of 0.7 in $\eta - \varphi$ was saved in the file.

To try to find hadronic showers in the data, the variable D was tried, where D is the natural logarithm of the ratio of post-shower energy to the energy in the SMD,

$$D = \ln [E_{Post}/(E_{Usmd} + E_{Vsmd})] .$$

Hadronic showers take longer to develop so they are expected to have a lot of post-shower energy. On the other hand the electromagnetic showers are expected to be mostly contained in the towers. We compare events with an identified charged particle and

events where no charged particle is identified in the kinematic region where there is good TPC tracking (1.1 < eta < 1.4). In Fig. 41 below, there is a greater concentration of events at values of D > -4 when there is a charged track compared to the case of no charged track. This is even clearer looking at Fig. 42, which is the ratio of Figs. 41b and 41a.

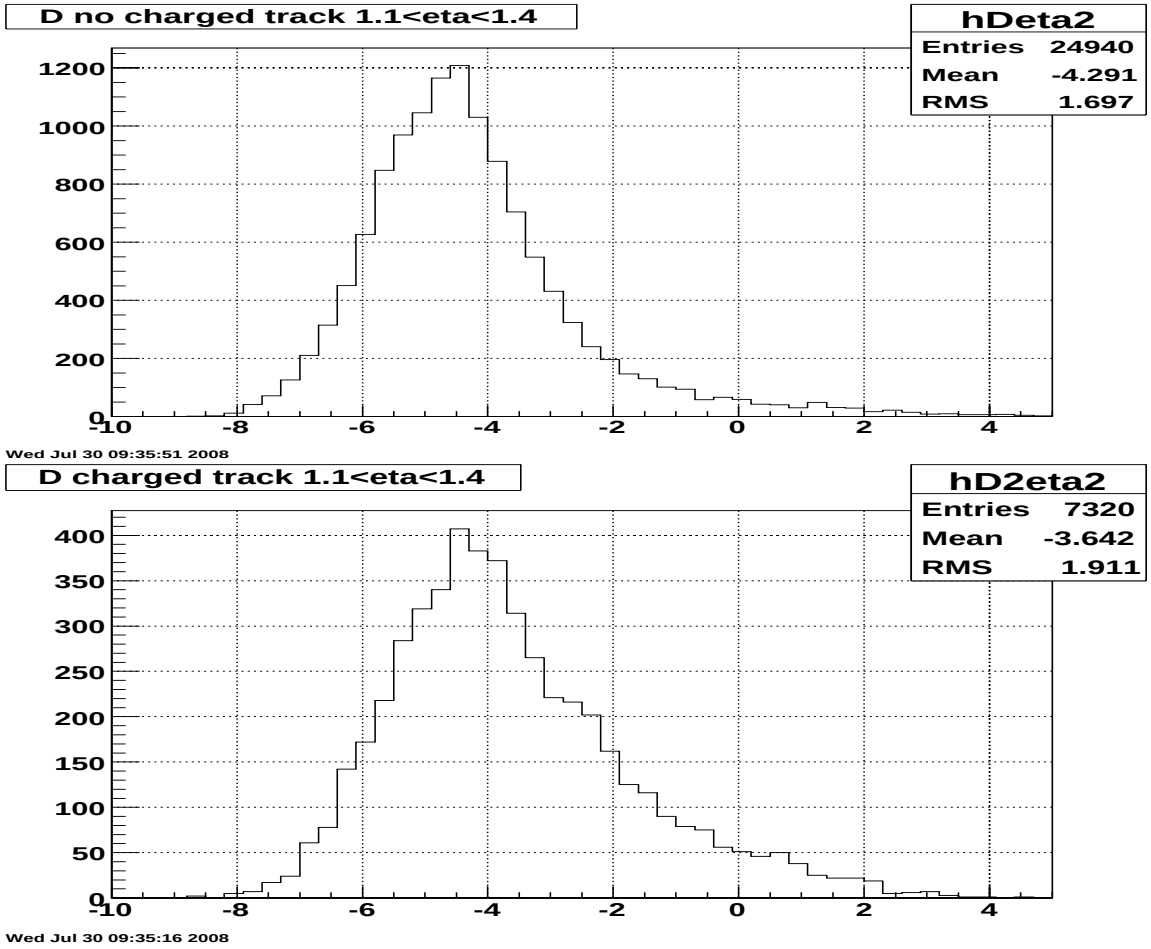

Fig. 41. A comparison of the parameter D for events that have no charged track (upper), and those that have charged tracks (lower).

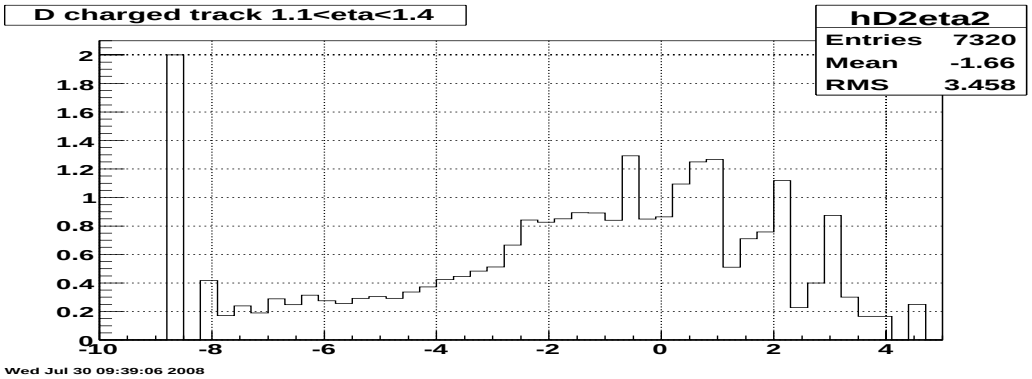

Fig. 42. The ratio of Figs. 41b to 41a is plotted.

Tracking for larger values of pseudo-rapidity is limited, so we can not study charged showers with any statistical significance for larger values of eta; see Fig. 43.

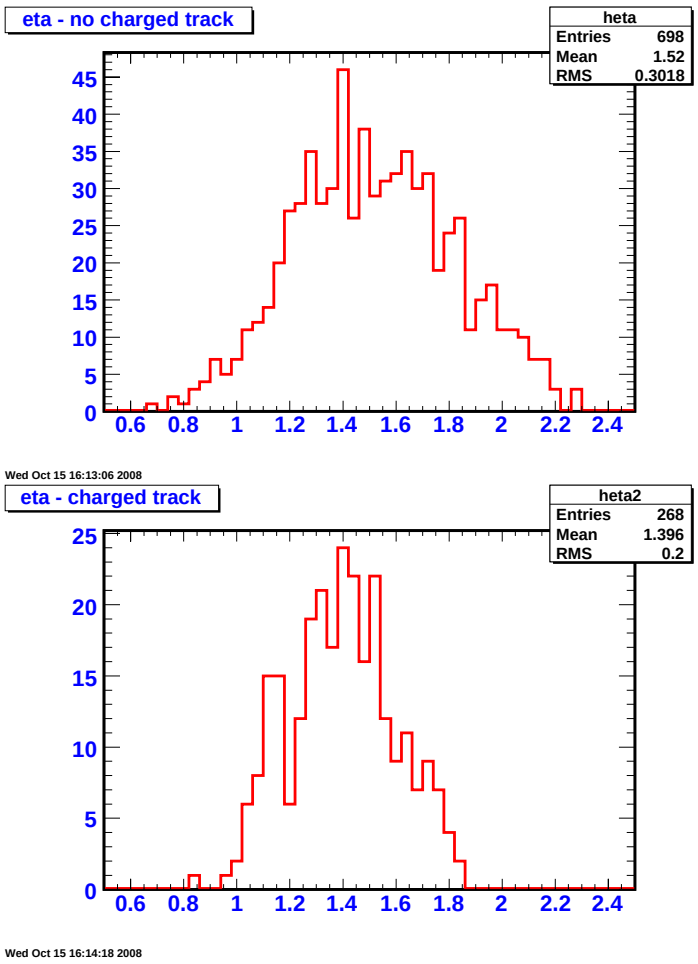

Fig. 43. Eta distribution for events without charged tracks (above) and for events with charged tracks (below).

The 4 plots below in Fig.44 contain histograms of D for different pre-shower conditions with no charged track. If we take the pre-shower information from Fig. 44 at face value then the purest electromagnetic showers should be when both E_{Pre1} and E_{Pre2} are greater than zero. The samples most contaminated with hadronic showers should be when E_{Pre2} is zero and E_{Pre1} is zero or greater than zero. Histograms 44b and 44d are very similar except that the average is shifted to the right for 44b, which makes sense because it would correspond to a later-starting shower ($E_{Pre1} = 0$). The distributions on the left are

clearly different than the ones on the right. The means are very different and the shapes are also very different. If we tried to interpret the difference between Figs. 44c and 44d as due to inefficiency in pre-shower2 then that inefficiency would be about 1.7% (100% x 310/18417). However, inefficiency in pre-shower2 would produce the same shaped distribution, which is not observed.

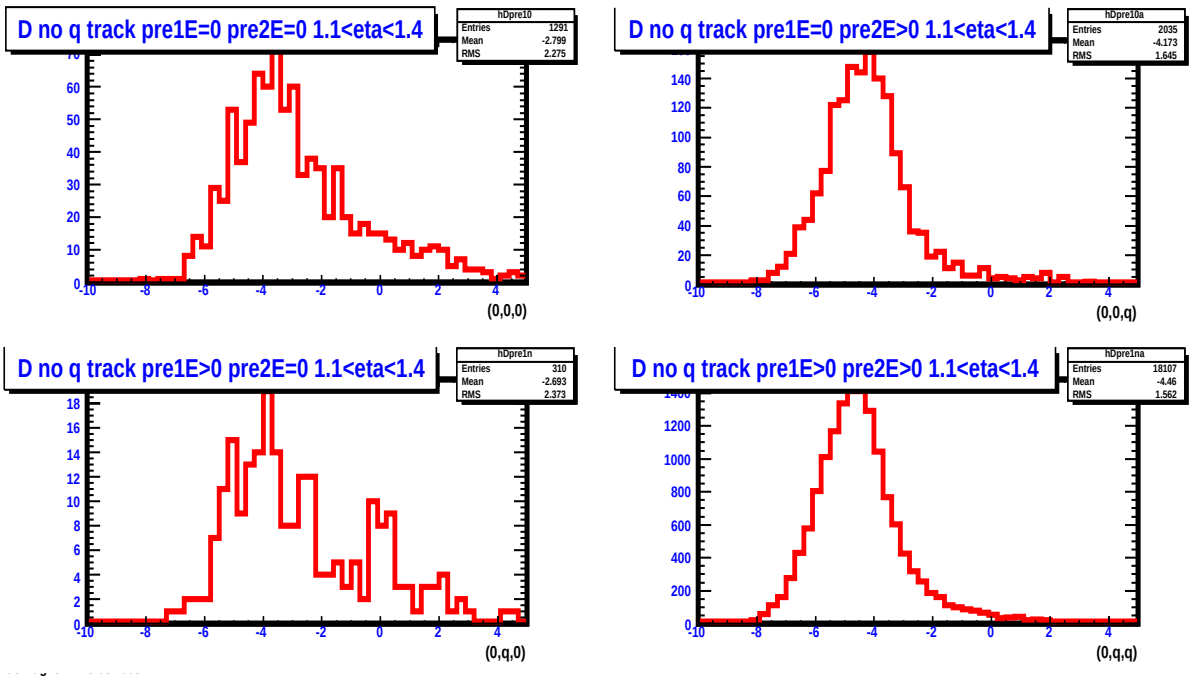

Fig. 44. All histograms require no charged tracks. a(upper left): both E_{Pre1} and E_{Pre2} are zero. b(upper right): $E_{Pre1} = 0$ and $E_{Pre2} > 0$. c(lower left): $E_{Pre1} > 0$ and $E_{Pre2} = 0$. d(lower right): $E_{Pre1} > 0$ and $E_{Pre2} > 0$.

The pre-shower conditions for Fig. 44c imply a very unusual event. A neutral particle leaves the interaction region, converts to a charged particle before pre-shower1 and then becomes neutral before pre-shower 2. This is indicated on the diagram by the compact notation (0,q,0) → (no charge leaving the interaction region, charge at Pre1, and no charge at Pre2).

Figure 45 has similar plots to Fig. 44, but in this case there is an identified charged track. In each case the mean and the shapes are different than when there is no charged track. The number of events is low except for Fig. 445, where E_{Pre1} and E_{Pre2} are both greater than zero. Figure 45d has a very pronounced tail towards large D.

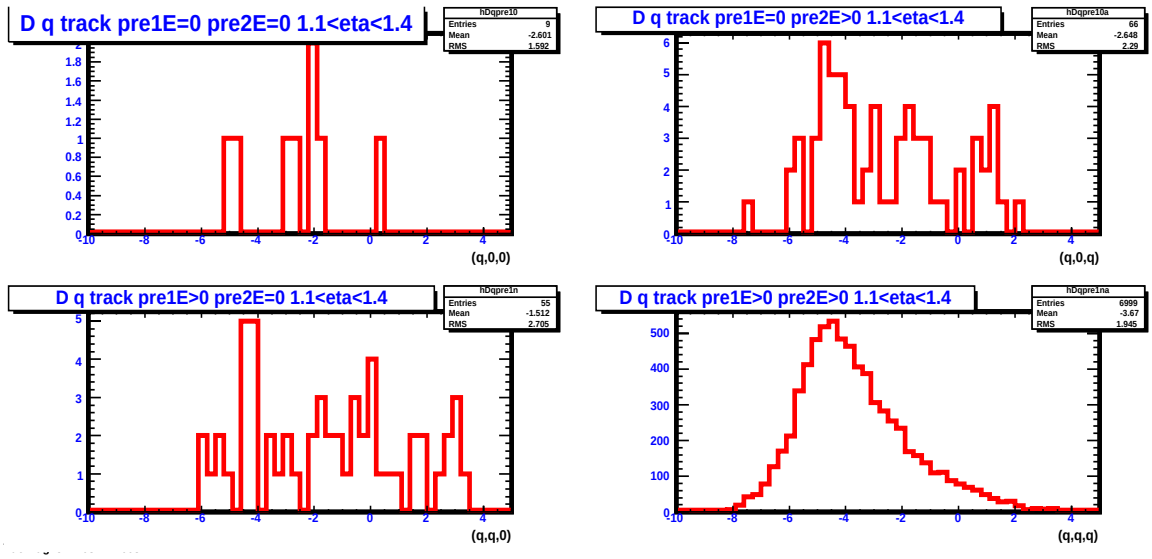

Fig. 45. This is the same as Fig. 44 except there is an identified charged track.

In another attempt at finding some means of identifying hadronic events we define a new variable,

$$\text{Dtower} = \ln [E_{Post}/(E_{tower})].$$

This compares the post-shower energy with the tower energy. For hadronic events one would expect more post-shower energy. Figures 46 and 47 contain 8 plots with all the same variations in pre-shower conditions that were given for the original D. There appears to be no better distinguishing characteristics in Dtower than in the original D.

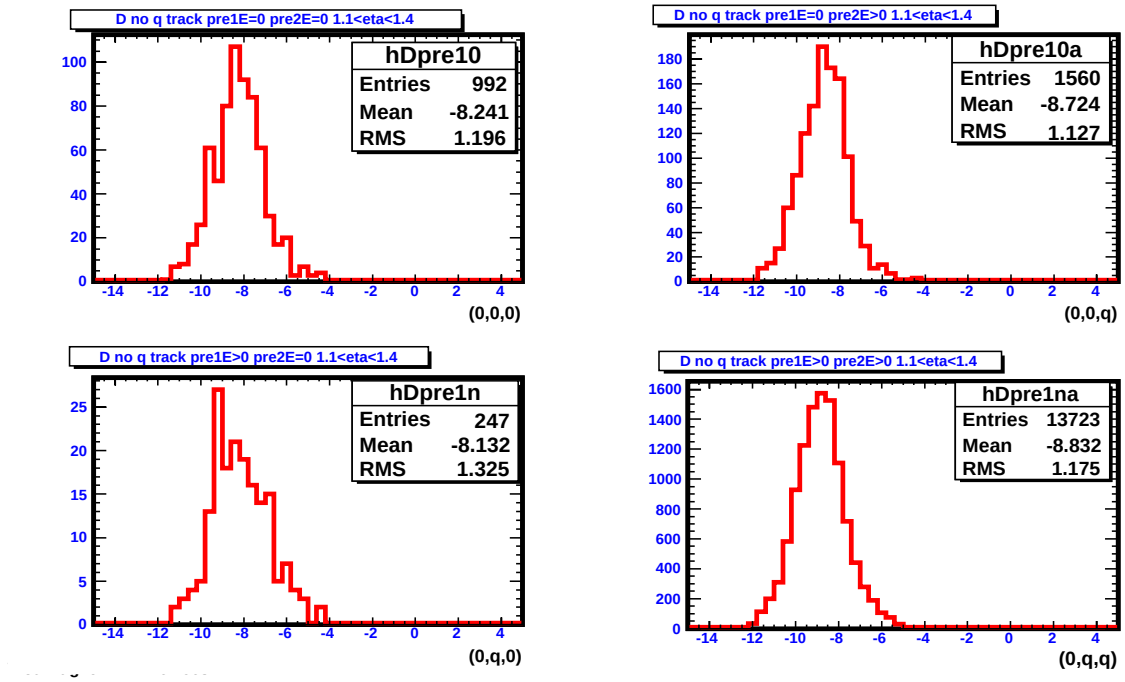

Fig. 46. Same conditions as in Fig. 44 except that D is now replaced by Dtower.

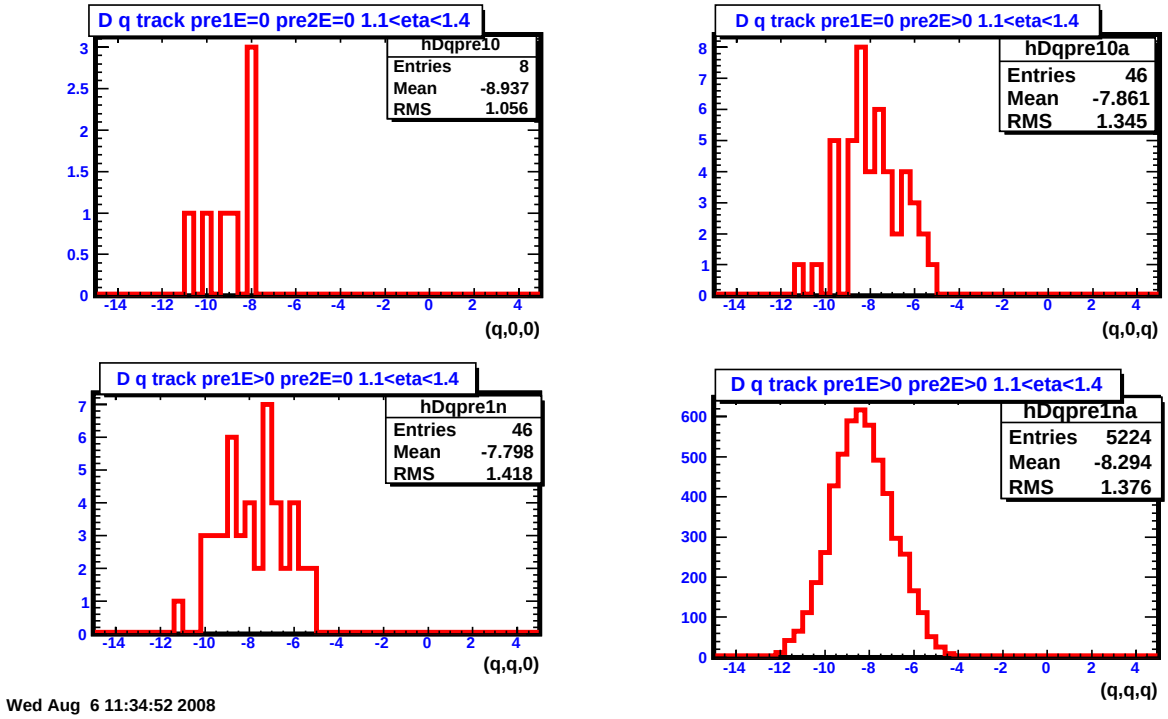

Fig. 47. Same conditions as in Fig. 45 except that D is now replaced by Dtower.

The SMD shower shapes were compared for events with and without charged tracks pointing to the cluster. The U and V shapes were consistent for all cases. It was observed that the widths were slightly narrower for the case without charged tracks (3.74[U], 3.78[V] ± 0.13 vs. 3.91, 3.87 ± 0.24 strips); see Fig. 48. Requiring $E_{Post} > 10$ MeV resulted in slightly narrower shower widths (3.46, 3.38 ± 0.59 vs. 3.67, 3.66 ± 0.58 strips, respectively). The distribution of the number of non-zero energy strips is somewhat different for the charged and no-charged cases – see Fig. 49. Finally, the summed SMD energy within ±12 strips of the energy weighted mean strip is slightly less for showers with a charged track than without a track, as shown in Fig. 50.

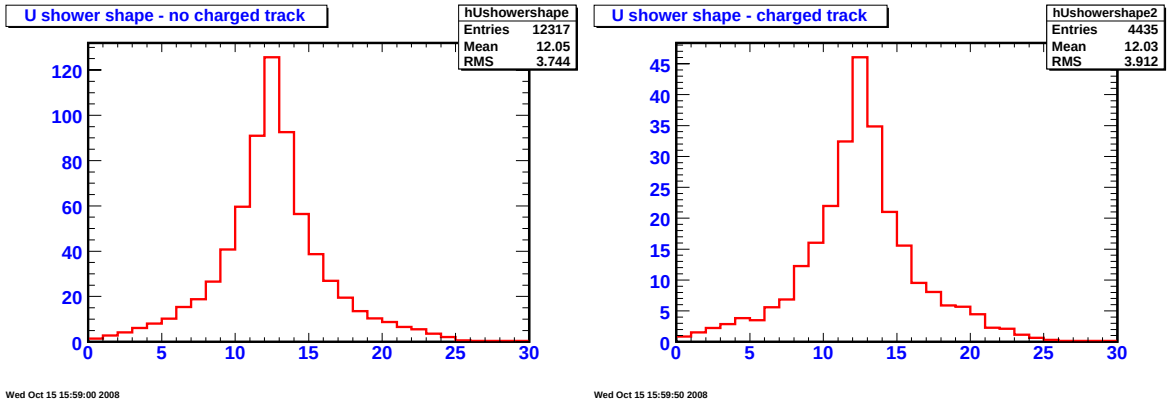

Fig. 48. Average SMD shower shapes for the case without (left) and with (right) charged particles pointing toward the shower are shown.

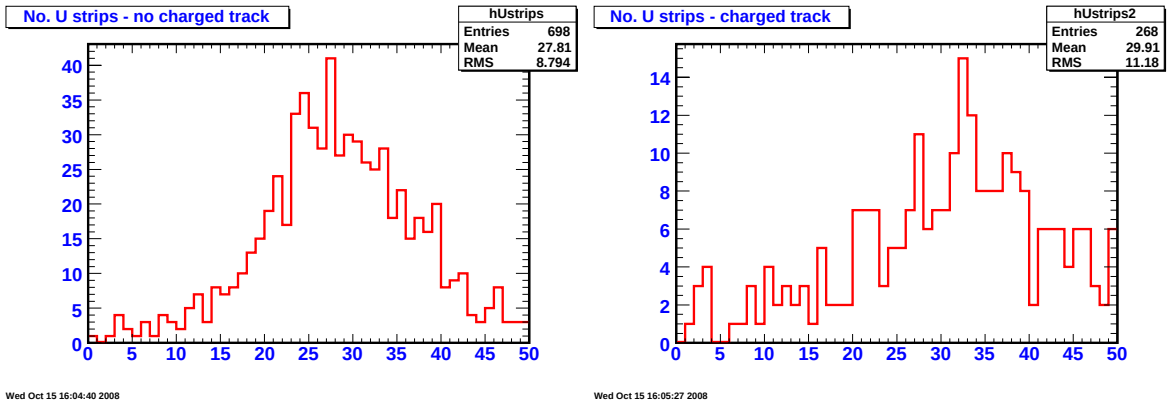

Fig. 49. The distributions of the total number of non-zero energy SMD strips per sector for cases without (left) and with (right) charged particles pointing toward the shower are shown. Note the means are both larger than 25, which is the number of strips typically used to evaluate shower shapes in this note.

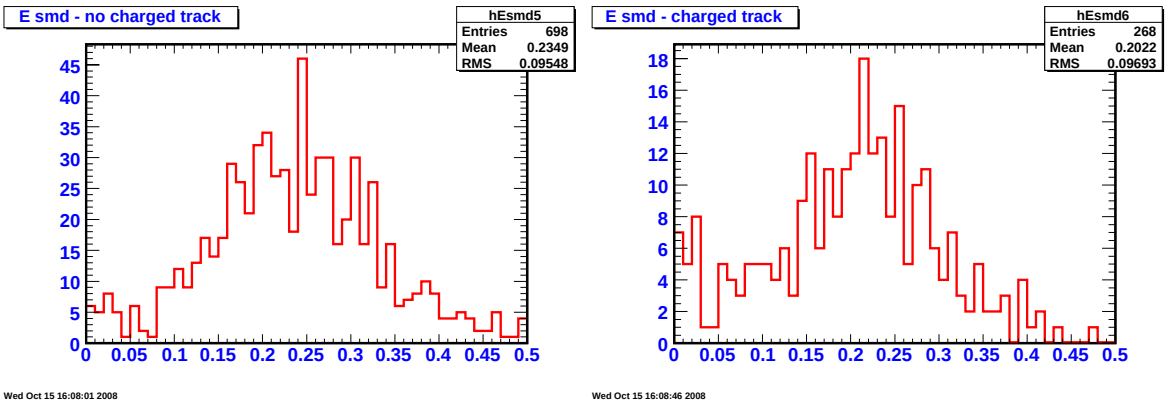

Fig. 50. The distributions of summed SMD energy within ±12 strips of the energy weighted mean strip is plotted for the cases without (left) and with (right) charged particles.

6. Summary

A summary of some of the findings from the studies reported in this paper follows:

- From the evaluation of individual $\eta \rightarrow \gamma\,\gamma$ candidates by Pibero:
  - Will's selection of events gave less pre-shower1 energy on average than the full sample of candidates (Fig. 1).
  - There was a correlation of the number of pre-shower1 counters with non-zero energy and the number of towers with non-zero energy in a sector (Fig. 2).
  - Isolated "mip" or larger events (backgrounds?) are distributed approximately uniformly in the EEMC (Fig. 3).
- From studies of Pibero's 927 photon candidates from $\eta \rightarrow \gamma\,\gamma$ decay:
  - The events are concentrated near tower centers (Fig. 5).
  - There is a correlation between the total sector SMD energy sums E_U and E_V (Fig. 6).
  - The SMD shower widths increase with E_{Pre1} and decrease with shower energy for $E_{Pre1} = 0$ (Fig. 9).
- Using Will's 3334 photon candidates from $\eta \rightarrow \gamma\,\gamma$ decay:
  - There is a correlation between the total sector SMD energy sums E_U and E_V (Fig. 12), but it appears wider than observed for Pibero's photon candidates. Also, there is a correlation when summing over ±12 strips from the SMD cluster center, and it is weaker still (Fig. 12).
  - The SMD shower widths get broader with depth of the SMD in the EEMC. This is consistent with Pibero's result, which had less statistical significance.
  - Information from both photons from η decay is retained in Will's sample. The invariant mass of the two photons shows a significant background beneath the η peak (Fig. 13).

- The $z_{\gamma\gamma}$ distribution is peaked near 0.5-0.6 (Fig. 13), which probably leads to the double peaks in the E_{tower} and E_{trans} distributions (Fig. 10).
- The shower shapes for Pibero's and Will's candidates are very similar (Fig. 14). The shape changes very little with energy, but the RMS variation decreases with energy (Fig. 15).
- The SMD shower widths increase slightly with pseudo-rapidity, as expected from geometric effects (Fig. 16).

- Comparisons to Ilya's γ + Jet inclusive candidate data and Monte Carlo simulations for these inclusives indicated:
  - The fraction of events with $E_{Pre1} = 0$ was about 0.4 for Pibero's and Will's candidates, 0.3 for the Monte Carlo events, and 0.06 for Ilya's data. Two possible explanations include considerable additional material in the actual detector compared to simulations, or the dominance of processes other than γ + Jet inclusives in the recorded data.
  - The conversion probability between the pre-shower1and preshower2 counters was about 0.56 for Will's and Pibero's candidates, 0.60 for the Monte Carlo events, and 0.77 for Ilya's data. The behavior as a function of pseudo-rapidity matched simple calculations based on the known material and geometry for Will's photon candidates, but disagreed for Ilya's events (Fig. 17). One possibility is that Ilya's sample contains a significant number of particles other than or in addition to photons.
  - The average ratio of SMD energy within ±12 strips of the maximum energy strip to the 3 × 3 tower cluster energy was largest for Will's and smallest for Ilya's events for a given number of non-zero SMD strips (Figs. 19 – 22) while the opposite was true for the ratio of post-shower to tower energy (Fig. 23). Ilya's events had more non-zero strips on average.
  - Will's photon candidates had approximately the same shower shape and RMS variation for three pre-shower conditions (Fig. 24). Reduced chi-squared distributions for Will's events with energy larger than 8 GeV also were approximately independent of pre-shower counter conditions, while Ilya's events showed considerable differences (Figs. 25, 26). In particular, it appears difficult to select single photons from Ilya's sample when the pre-shower1 counter energy is larger than 5 – 10 MeV.
  - Will's photon candidates have a left-right asymmetry that changes with photon energy and pseudo-rapidity (Figs. 27, 28). One source may be changing SMD strip lengths across the sector, but this does not appear to be the full explanation for the observed behavior.
- Estimating the amount of material from the photon conversions before the pre-shower1 counter from Will's photon candidates:
  - There is a significant enhancement in the number of events near the edge of sectors for $E_{Pre1} = 0$ and a smaller enhancement for $E_{Pre1} > 0$ (Fig. 29).
  - No significant structure was observed on a finer scale within a sector for either $E_{Pre1} = 0$ or > 0 photon candidates (Figs. 33 – 35).
  - The derived amount of material, in radiation lengths, appears to have minima near the center of a sector in φ and near Y ~ 240 cm (Fig. 36).

The effect of TPC supports in sectors 3 and 9 may have been observed in Fig. 37.

- The derived amount of material is generally largest for the lowest energy photons, perhaps indicating multiple photons or particles present in the 3 × 3 pre-shower1 cluster.

- Studies of different events from Pibero with charged particle information from the TPC indicated:
  - There were additional events at larger ratios of post-shower to SMD energy for charged compared to no charged tracks pointing to the 3 × 3 cluster (D parameter – Figs. 41, 42).
  - The detailed shapes of the D-distributions for various pre-shower and charged vs. no-charged conditions are not understood (Figs. 44, 45).
  - The ratio of post-shower to tower energy in Figs. 46 and 47 does not seem to show significant changes with pre-shower or charged vs. no-charged conditions.
  - Relatively small differences were observed in the SMD shower shapes, number of non-zero energy strips per sector, or total summed SMD energy for cases with or without charged tracks pointing to the shower.

Acknowledgements:

We wish to thank Pibero Djawotho, Will Jacobs, Ilya Selyuzhenkov, Jason Webb, Scott Wissink and other STAR collaborators for assistance in these calculations and helpful discussions. This work was supported in part by the United States Department of Energy, Office of Science, Division of Nuclear Physics.

References

1. K.H. Ackermann et al., Nucl. Instrum Meth. A499, 624 (2003).
2. C.E. Allgower et al., Nucl. Instrum. Meth. A499, 740 (2003).
3. The description of the selection of these photons is given by P. Djawotho in http://www.star.bnl.gov/protected/spin/pibero/photons/etas
4. http://www.star.bnl.gov/protected/spin/pibero/photons/etas/eta_all_sectors.pdf
5. The description of the event selection is given by P. Djawotho in http://www.star.bnl.gov/protected/spin/pibero/photons/etas2
6. The description of the event selection is given by W. Jacobs in http://www.star.bnl.gov/protected/spin/wwjacobs/GAMMA/etas_2
7. S. Wissink, private communication.
8. F. Abe et al., Phys. Rev. D48, 2998 (1993).
9. L. Nakae, Ph.D. thesis, Brandeis University (1992).
10. A description of the two large LHC detectors is given in http://indico.cern.ch/conferenceDisplay.py?confId=a07193
11. The data were saved by P. Djawotho on the BNL data analysis computers as root files under /star/institutions/iucf/pibero/2006/gamma/Trees.

High Energy Physics Division
Argonne National Laboratory
9700 South Cass Avenue, Bldg. 362
Argonne, IL 60439-4815

www.anl.gov

A U.S. Department of Energy laboratory
managed by UChicago Argonne, LLC